Numerical investigation of the effects of roughness, a berm and oblique waves on wave overtopping processes at dikes

Chen, W.; Warmink, J.J. ; van Gent, M.R.A.; Hulscher, S.J.M.H.

DOI
10.1016/j.apor.2021.102971

Publication date
2022

Document Version
Final published version

Published in
Applied Ocean Research

Applied Ocean Research 118 (2022) 102971

Contents lists available at ScienceDirect

Applied Ocean Research

journal homepage: www.elsevier.com/locate/apor

Numerical investigation of the effects of roughness, a berm and oblique waves on wave overtopping processes at dikes

W. Chen [a,b,*], J.J. Warmink [a], M.R.A. van Gent [b,c], S.J.M.H. Hulscher [a]

[a] Department of Marine and Fluvial Systems, University of Twente, 7522 NB, Enschede, the Netherlands
[b] Department of Coastal Structures & Waves, Deltares, 2629 HV, Delft, the Netherlands
[c] Department of Hydraulic Engineering, TU Delft, 2628 CN, Delft, the Netherlands

ARTICLE INFO

Keywords:
OpenFOAM®
Overtopping flow velocity
Layer thickness
Overtopping discharge
Two-dimensional numerical model
Three-dimensional numerical model
Oblique wave attack

ABSTRACT

The mean overtopping discharge and the overtopping flow parameters related to individual overtopping events are often used to characterize the wave overtopping processes at dikes. Roughness, berms and oblique waves have significant effects on the wave overtopping processes at dikes while these effects are still not fully understood. A 2DV OpenFOAM® model is validated using experimental data for predicting flow velocity and layer thickness at the waterside edge of the crest. The validated numerical model is then applied to investigate the effects of roughness and a berm on the flow velocity and layer thickness. The roughness is modelled by creating protrusions along the waterside slope. Numerical model outcomes indicate that existing empirical formulas underestimate wave overtopping quantities. Introducing a roughness factor to existing empirical formulas leads to better estimates of the flow characteristics. We found that the flow characteristics are more sensitive to the variation of the berm width than to the berm level. Model results demonstrate that existing formulas for predicting the flow characteristics, as derived based on smooth straight slopes, also work well for slopes with a berm. Rayleigh and Weibull distribution functions are derived to estimate the flow velocity and layer thickness with exceedance probabilities below 10%. In order to take oblique waves into account, the 2D numerical model is extended into the 3D model domain. This 3D OpenFOAM® model is validated using measured mean overtopping discharges. The influence of oblique waves on the mean overtopping discharge in combination with a berm is analysed. The numerical model computations confirm that the reductive influence factor of oblique waves is dependant on the berm width.

1. Introduction

Wave overtopping is one of the main causes of dike breaching. Therefore, wave overtopping has to be taken into account for the design and safety assessment of dikes. Wave overtopping at dikes is usually characterized by the mean overtopping discharge and by the overtopping flow parameters such as flow velocity and layer thickness related to individual overtopping events. Previous failure analyses demonstrated that dike failures at the landside slope are mainly caused by individual overtopping events, particularly by the related overtopping flow velocities and layer thicknesses (Schüttrumpf, 2001; Van Gent, 2002a, 2002b; Schüttrumpf and Van Gent, 2003; Schüttrumpf and Oumeraci, 2005). Thus, for flooding events initiated by dike breaching due to wave overtopping, overtopping flow velocities and layer thicknesses are more important than average overtopping discharges since the average overtopping discharge does not account for the effects of extreme individual overtopping events. However, the average overtopping discharge is still important as it is often used to determine the crest height of coastal structures. Nowadays, risks of coastal flood disasters are increasing as a result of climate change, sea level-rise and land subsidence (Temmerman et al., 2013). Against this background, some existing dikes may require reinforcement and adaption (Van Gent, 2019). Berms and roughness elements at the seaside slopes of dikes are widely applied to reduce wave overtopping quantities. In practice, the direction of incoming waves in many circumstances is not perpendicular to the structure (Van Gent, 2021). Existing guidelines show that berms, roughness and oblique waves at the waterside of the dike have significant effects on wave overtopping processes. Therefore, the reductive effects of berms, roughness and oblique waves should be taken into account when predicting the wave overtopping quantities at dikes.

* Corresponding author.
E-mail address: w.chen-6@utwente.nl (W. Chen).

https://doi.org/10.1016/j.apor.2021.102971
Received 22 June 2021; Received in revised form 4 November 2021; Accepted 15 November 2021
Available online 24 November 2021

Table 1
Empirical coefficients for calculating the 2%-values of flow velocity and layer thickness at the waterside edge of the dike crest, in which α [°] is the angle of the waterside slope of a dike.

	Waterside slope	$c_{v2\%}$	$c_{h2\%}$	a	b
Van Gent (2002a)	1/4	1.3	0.15	1	1
Schüttrumpf (2001)	1/6	1.37	0.33	0	1
EurOtop (2018)	1/3–1/5	1.4–1.5	0.2 for slopes of 1/3 and 1/4; 0.25 for a slope of 1/5; 0.3 for a slope of 1/6	0	1
Formentin et al. (2019)	1/4, 1/2	0.12cot(α)+0.41	0.085cot(α)	0	1.35

Extreme conditions, i.e. flow velocity and layer thickness with a low probability of exceedance during a storm event, are usually used to characterize the wave overtopping flow. The overtopping flow velocity and layer thickness at the waterside edge of a dike crest also provide important boundary conditions for the estimation of wave loading parameters along the crest and at the landward slope. For example, the analytical and numerical models (Van Bergeijk et al., 2019, 2020) for predicting the flow parameters along the crest and landward slope both require estimates of the flow velocity and layer thickness at the waterside crest as the model input. Several predictors are available to estimate the extreme overtopping flow characteristics at the seaward edge of a dike crest. Schüttrumpf (2001) and Van Gent 2002a, 2002b used theoretical and experimental investigations to develop empirical formulas for extreme overtopping flow velocity and layer thickness exceeded by 2% of the incoming waves. The results were later combined in Schüttrumpf and Van Gent (2003). EurOtop (2018) also provide empirical equations for estimating the 2%-values of flow velocity and flow thickness. Formentin et al. (2019) performed numerical model computations and proposed formulas based on those by Schüttrumpf (2001) and Van Gent (2002a) for estimating flow characteristics at the waterside edge of the dike. Mares-Nasarre et al. 2019, 2021 extended the formulas given in Schüttrumpf and Van Gent (2003) for estimating the overtopping flow velocity and layer thickness for applications on rubble mound breakwater crests.

Most of the empirical equations for the extreme flow velocity and layer thickness at the seaward edge of the dike crest are estimated using the following shape:

$$\boldsymbol{u}_{2\%} = \boldsymbol{c}_{v2\%}\left[\sqrt{\boldsymbol{g}(\boldsymbol{R}_{u2\%} - \boldsymbol{R}_c)\Big/\boldsymbol{\gamma}_f^a}\right]^b \tag{1}$$

$$\boldsymbol{h}_{2\%} = \boldsymbol{c}_{h2\%}\left[(\boldsymbol{R}_{u2\%} - \boldsymbol{R}_c)\Big/\boldsymbol{\gamma}_f^a\right]^b \tag{2}$$

where $c_{v2\%}$, $c_{h2\%}$ and b are empirical coefficients; R_c [m] is the freeboard which represents the crest level relative to the still water level (SWL); $R_{u2\%}$ [m] is the wave run-up height exceeded by 2% of the incoming waves, which can be estimated using Eq. (A. 1) proposed by Van Gent (2001) or Eqs. (A. 2) & (A. 3) as given in EurOtop (2018). Herein, γ_f [-] is the influence factor of slope roughness. The roughness influence factor γ_f is only included in the Van Gent (2002a) equations corresponding to $a = 1$; γ_f is not included (which means a is equal to 0) in other existing empirical formulas. Values of the empirical coefficients $c_{v2\%}$ and $c_{h2\%}$ provided in previous research are not consistent (see Table 1). The differences could be explained by different dike configurations, experimental instruments and procedures of determining the 2% values of flow parameters. Even though there is extensive literature on the overtopping flow characteristics at dikes, previous research mainly considered the dike configurations with smooth straight waterside slopes. It still remains unclear if the existing formulas are also applicable for predicting the flow characteristics over dikes that have a rough waterside slope with or without a berm.

Apart from the overtopping flow velocity and layer thickness, estimates of the mean overtopping discharge still play an important role in the design and safety assessment of coastal structures. TAW (2002) and EurOtop (2018) provide overtopping equations which are widely used around the world, taking several influence factors (i.e. berms, roughness, oblique waves, vertical wall) into account. A lot of research (e.g. De Waal and Van der Meer, 1992; Capel, 2015; Van der Werf and Van Gent, 2018; Schoonees et al., 2021) has been conducted on each of these influence factors. Chen et al. (2020a; 2020b) studied the effects of the roughness in combination with a berm on overtopping discharges and proposed empirical equations based on the analysis of experimental results. Van Gent (2020) studied the effects of roughness and a berm in combination with oblique waves by means of physical model tests. An empirical equation to account for effects of oblique waves was proposed, in which an assumption was made that the influence factor of oblique waves was dependant on the berm width. However, this assumption has not been verified for various berm widths. Verification of this assumption is important for accurately predicting the mean overtopping discharge when oblique waves and a berm are present at the same time.

Above all, the applicability of the existing formulas for estimating the overtopping flow characteristics at the waterside edge of the dike crest to dikes that have a bermed or rough waterside slope still remains unknown. Additionally, the dependency of the oblique wave influence on the berm width requires verification. Therefore, the objective of this study is the investigation of the effects of a berm, roughness and oblique waves on wave overtopping processes at dikes.

For that purpose, the 2DV OpenFOAM® model by Chen et al. (2021), which has been validated for predicting the overtopping discharge at dikes, is applied in this study. Physical model tests presented in Van Gent (2002a) were used to validate this 2DV OpenFOAM® model for flow velocities and layer thicknesses at the waterside edge of the dike crest. Following that, the validated numerical model is applied to investigate the effects of roughness and a berm on the overtopping flow characteristics. A verification of the existing empirical formulas will be provided. Then, the 2DV numerical model is further extended into a 3D numerical model to take the oblique waves into account which is first validated using the experiments from Van Gent (2020). The berm width is varied with the incident wave angle fixed at 30° in the 3D numerical tank. Herein, the incident wave angle is defined as the angle between the direction of incident waves and the perpendicular to the long axis of the dike. The influence of oblique waves on the mean overtopping discharge for different berm widths is analysed to check the dependency of the influence factor of oblique waves on the berm width.

The paper is organized as follows. The methodology is described in Section 2. In Section 3, the validation of the 2D and 3D numerical models is presented. Section 4 is focused on the applications of the numerical models to study the effects of roughness, a berm and oblique waves on flow characteristics and overtopping discharges. In Section 5, the numerical model results are further discussed followed by the conclusions in Section 6.

2. Methodology

In this section, the applied method for the 2D numerical modelling is first introduced, including a brief description of the 2D experiments that are used to validate the 2D numerical model. Then, the numerical model set-ups are introduced followed by the numerical experiments for studying the effects of roughness and a berm on overtopping flow parameters. Hereafter, the method for the 3D numerical model is introduced in a similar way.

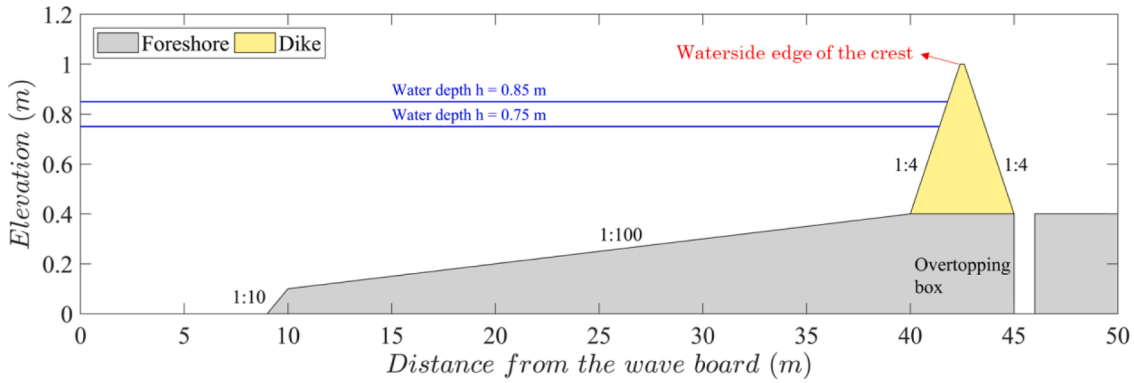

Fig. 1. Set-up of the physical model (adapted from Van Gent, 2002).

Table 2
Selected cases with wave conditions and measured results at the waterside edge of the dike crest from Van Gent (2002a).

Test	h_deep	h_toe	H_{m0} [m]	$T_{m-1,0}$ [s]	$h_{2\%}$ [m]	$u_{2\%}$ [m/s]
T101	0.75	0.35	0.149	2.16	0.0143	1.53
T102	0.75	0.35	0.142	1.84	0.0058	0.99
T103	0.8	0.4	0.153	2.14	0.0212	1.74
T104	0.85	0.45	0.147	1.78	0.0204	1.64
T201	0.8	0.4	0.152	2.03	0.016	1.55
T202	0.8	0.4	0.148	1.92	0.014	1.53
T203	0.8	0.4	0.139	1.84	0.0117	1.44
T204	0.8	0.4	0.13	1.86	0.0101	1.29
T205	0.8	0.4	0.142	1.69	0.0076	1.09
T206	0.8	0.4	0.138	1.62	0.0076	1.08

2.1. numerical modelling

2.1.1. Description of 2D physical tests

The small-scale physical model tests in Van Gent (2002a) were performed in the Scheldt Flume at Deltares in the Netherlands. The flume has a length of 55 m and a height of 1.2 m. A foreshore with a slope of 1:100 over a length of about 30 m was applied as shown in Fig. 1. A step with a 1:10 slope was constructed between the wave board and the start of the foreshore to obtain a sufficient depth at the wave board. The distance between the toe of the structure and the wave board was 40 m. The dike configuration with a slope of 1:4 is shown in Fig. 1. The slopes were smooth. The bottom elevation at the toe was 0.4 m and the crest elevation was 0.6 m above the bottom at the toe.

Three wave gauges were installed near the toe to measure the surface elevation. The incident waves at the toe were determined by repeating the tests with the foreshore but without the structure in position using the method by Mansard and Funke (1980). The position at the waterside edge of the crest was measured. The overtopping flow velocity was measured using a velocity metre which was a propeller with a diameter of approximately 10 mm. It was capable of measuring velocities in the range of 0.5 m/s to 4 m/s for water-layers with a thickness larger than 2 mm. The devices for measuring the layer thickness were accurate with the error smaller than 0.2 mm between 1 and 100 mm.

Ten tests were selected to validate the 2DV OpenFOAM® model as presented in Table 2. The water depth at the toe varied between 0.35 m and 0.45 m. The irregular waves in tests T101∼T104 were generated based on the TMA-spectra (Bouws et al., 1985). Tests T201∼T206 were performed with double-peaked wave energy spectra which were obtained by superposition of two single-peaked TMA spectra.

2.1.2. numerical model set-up

The 2DV OpenFOAM® model by Chen et al. (2021) was applied in this study with the layout of the model adapted according to the physical tests in Van Gent (2002a). The length of the domain of the 2D physical tests was about 45 m. Simulating the entire domain in an OpenFOAM® model would be computationally expensive. In order to save computational time, a part of the domain between 0 m and 28 m from the wave board was simulated in the OceanWave3D which is a computationally cheaper solver. The rest of the domain was simulated in the OpenFOAM® model as shown in Fig. 2. Since the flow characteristics are closely related to the wave run-up height according to previous literature, the wave run-up height was also simulated using the numerical model. In order to obtain wave run-up heights, a different dike configuration was modelled, in which the seaward slope was extended until the crest elevation reached 1.35 m such that no waves could overtop the crest. A constant pressure was applied at the atmosphere boundary which allowed the air to flow in and out and allowed the water to only flow out. The boundaries of the modelled impermeable structures and flume bottom were set as non-slip conditions. The turbulence was

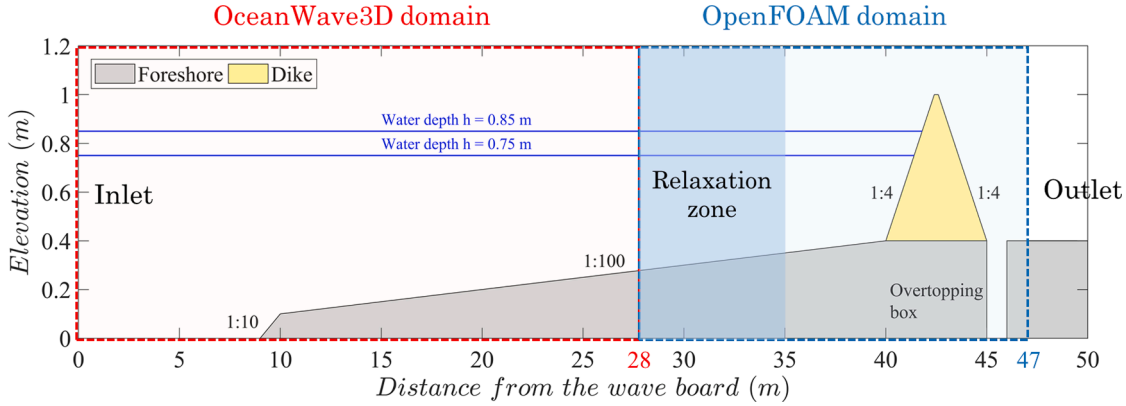

Fig. 2. Numerical domains for OceanWave3D model and OpenFOAM® model. .

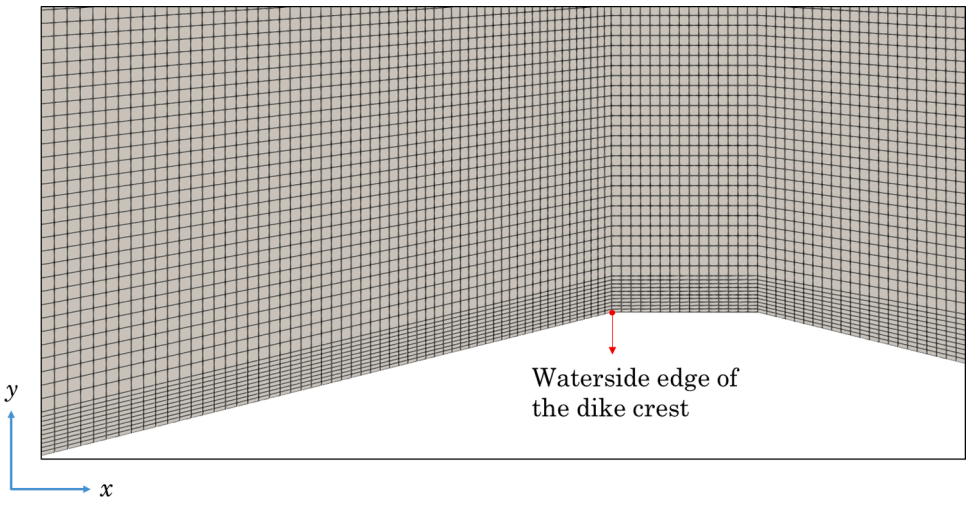

Fig. 3. Mesh around the structure in the 2D OpenFOAM® model with the grid size Δy=0.005 m near the crest.

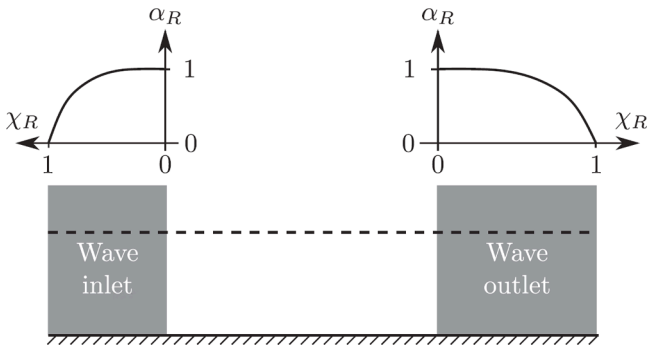

Fig. 4. Variation of $\alpha_R(\chi_R)$ in relaxation zones (from Jacobsen et al., 2012). .

accounted for by applying a stabilized $k-\omega$ turbulence model developed by Larsen and Fuhrman (2018). Each simulation was made lasting about 600 s, resulting in 280~350 waves depending on the wave period. This time duration was adopted to compromise the computational effort and the accuracy of the model results (Chen et al., 2021).

2.1.2.1. Mesh. The numerical mesh was created by using blockMesh which is a mesh-generation tool implemented in the OpenFOAM®. The base mesh from the inlet boundary to the toe of the dike was orthogonal and conformal with grid size of 0.026 m × 0.026 m. The grids near the free water surface were refined to 0.013 m × 0.013 m, which yielded about 12 cells in vertical to resolve per wave height and was sufficient for modelling the wave propagation as shown in Chen et al. (2021). Quadrilateral grids parallel with the slope surface were created in the area where the structure located as shown in Fig. 3. The mesh near the structure was refined by applying ten layers of cells resulting in the grid size of 0.005 m in y direction.

2.1.2.2. Wave generation. The waves2Foam toolbox developed by Jacobsen et al. (2012) was applied to generate and absorb waves using relaxation zones within the OpenFOAM® model. The relaxation technique is an extension to Mayer et al. (1998) and a relaxation function is applied inside the relaxation zone

$$\boldsymbol{\alpha_R}(\chi_R) = 1 - \frac{\exp(\chi_R^{3.5}) - 1}{\exp(1) - 1} \quad \text{for } \chi_R \in [0;1] \tag{3}$$

in the following way

$$\phi = \boldsymbol{\alpha_R}\phi_{computed} + (1-\boldsymbol{\alpha_R})\phi_{target} \tag{4}$$

where ϕ represents the velocity field **u** or the water volume fraction α. α_R is always 1 at the interface (χ_R) between the relaxation zone and the non-relaxed part of the numerical domain and the relaxation function is illustrated in Fig. 4. Steering files of wave board motion based on the single-peaked or double-peaked TMA spectrum were first input to the OceanWave3D. The generated irregular waves in OceanWave3D provide the target solution ϕ_{target} for the inlet relaxation zone (also named coupling zone) of waves2Foam (for detailed information about the coupling method, reference is made to Paulsen et al., 2014). The length of the inlet relaxation zone was about one wave length as suggested by Jacobsen et al. (2012). Since the steering files were not the original files of the experiments, the generated time series of free surface elevation were not consistent with the experimental ones but the input wave properties including spectral significant wave height and spectral wave period were the same as those in the physical model tests.

2.1.2.3. Data postprocessing. The wave properties were determined using the results from three wave gauges defined near the position, where the toe of the structure was located. 30 probes were defined uniformly between 1.0 m and 1.05 m in vertical direction at the waterside edge of the crest in the OpenFOAM® model to detect the overtopping flow velocity and layer thickness. The water velocity at 5 mm above the crest (which corresponded to the centre of the velocity propeller) was extracted to represent the overtopping flow velocity. The layer thickness was determined based on the fraction indicator α [-]. $\alpha = 1$ means that a grid cell was totally filled with water. For the first cell with $\alpha < 1$ from the bottom up, the water thickness in this cell was calculated as $\Delta y * \alpha$ where Δy was the grid size in the vertical direction. The total water-layer thickness could then be determined by adding the thickness of all cells with $\alpha = 1$ and the thickness $\Delta y * \alpha$ in the first cell with $\alpha < 1$. In order to obtain the wave run-up height, 100 probes were defined uniformly along the extended waterside slope between $y = 0.55$ m and $y = 1.35$ m. The wave run-up heights were determined using the similar approach as that for layer thickness.

The tests listed in Table 2 were simulated and the numerically modelled wave properties and flow characteristics were compared with the experimental results for model validation. The Nash-Sutcliff model efficiency coefficient (NSE) is used to assess the predictive power of the OpenFOAM® model as is defined as follows:

$$\boldsymbol{NSE} = 1 - \frac{\sum_{i=1}^{N}(\boldsymbol{x_i} - \boldsymbol{y_i})^2}{\sum_{i=1}^{N}(\boldsymbol{x_i} - \overline{\boldsymbol{x}})^2} \tag{5}$$

where N is the number of measurements; x_i is the measured value and $\overline{x}$ is the mean value of the measurement data; y_i is the predicted value.

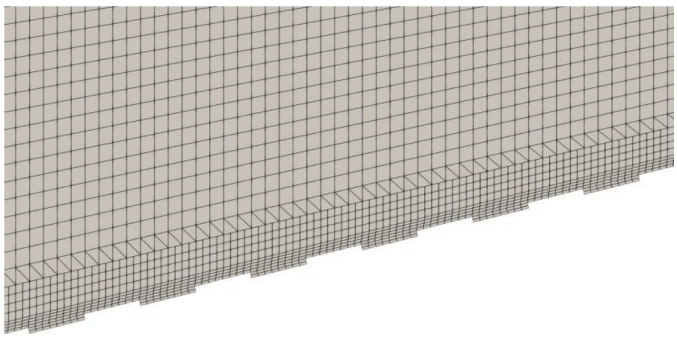

Fig. 5. Refined mesh around protrusions along the waterside slope.

$NSE = 1$ represents a perfect match of predicted values to the measured results. $NSE = 0$ means that the predicted results are as accurate as the mean of the measured results. $NSE < 0$ indicates that the mean value of the measured data is a better predictor than the numerical model.

2.1.3. Numerical experiments

The wave run-up height present in Eqs. (1) & (2) is the fictitious 2% wave run-up height. If the fictitious 2% wave run-up level is higher than the crest level, the roughness of the seaward slope is only effective up to the crest level and not up to the fictitious wave run-up level. However, the roughness reduction factor included in the formula for wave run-up (Eq. (A.1) or (A.2)) represented the roughness of the seaward slope effective up to the fictitious wave run-up level, the roughness factor was therefore included in Eqs. (1) & (2) suggested by Van Gent (2002) to correct for the effect of roughness between fictitious wave run-up level and the crest level. In contrast, other research assumed that the roughness influence was completely accounted by the wave run-up height and therefore it is not necessary to include the roughness influence factor in Eqs. (1) & (2). In order to check whether the roughness influence factor should or should not be included in Eqs. (1) & (2), the roughness was modelled by creating protrusions at the seaward slope as shown in Fig. 5. The protrusion height was 0.5 cm. For modelling the wave run-up height at the rough slope, the roughness was applied at the entire extended waterside slope which was often the case for determining the roughness factor in the physical experiments. Different wave conditions were simulated. The roughness factor was determined by comparing the wave run-up heights at a rough slope with those at a smooth slope ($\gamma_f = R_{u2\%-rough}/R_{u2\%-smooth}$). Simulated cases can be found in Table B.1.

The effect of a berm on the flow velocity and layer thickness was investigated by changing the berm width and the berm level relative to SWL. The berm width was changed in the range of 0 to 0.5 m (0 m, 0.1 m, 0.2 m, 0.3 m, 0.4 m, 0.5 m) and the berm level was varied in the range of 0.7~0.9 m (0.7 m, 0.75 m, 0.8 m, 0.85 m, 0.9 m) by changing the berm position with the water level fixed at 0.8 m. The two wave conditions W103 based on single-peaked TMA spectrum and W201 based on double-peaked TMA spectrum used in the validation cases T103 and T201 were applied here. The berm influence factor was determined by comparing the wave run-up heights at smooth slope with a berm to the run-up heights at a smooth straight slope ($\gamma_b = R_{u2\%-berm}/R_{u2\%-straight}$). Table B.2 presents the simulated cases for the investigation of the berm influence.

2.2. Numerical modelling

2.2.1. Description of 3D physical tests

The experiments from Van Gent (2020), which were used to validate the 3D numerical model, were performed in the Delta Basin (50 m × 50 m) at Deltares in the Netherlands. The layout of the model and tested cross-section are shown in Fig. 6. The angle between the long axis of the structure and the wave generator was 30°. The berm width was fixed at 0.3 m through the experiments. The overtopping measurements with smooth slopes were used in the present paper.

The irregular waves were generated based on a JONSWAP wave spectrum with a peak enhancement factor of 3.3. Waves were measured at 4 m distance from the toe of the structure. The overtopping water was collected using a chute guiding into the overtopping box. One wave gauge was installed in the overtopping box to measure the water surface elevation, based on which the volume of the overtopping water can be determined. The overtopping discharges were measured at four positions (q3 to q6) for the smooth slope as shown in Fig. 6a. The final average overtopping discharge were obtained using the mean values of the discharges at q3 to q6.

2.2.2. Numerical model set-up

In order to take the oblique waves into account, the 2DV OpenFOAM® model was extended with the second horizontal domain towards a 3D numerical model. Considering we are more interested in the trend of the oblique wave influence changing with the variation of the berm width than the accuracy of the absolute values of the numerically modelled average overtopping discharge, the 3D numerical model is used in a qualitative way. Additionally, the whole Delta Basin was too large to model in three dimension and therefore the size of the wave basin was reduced in the numerical model to compromise between the computational time and the model accuracy. The relaxation zone at the inlet was used to generate waves. Two relaxation zones were added at the side walls to absorb reflected waves from the structure. Fig. 7a presents an empty numerical basin which was used to calibrate the wave conditions in order to ensure the simulated wave conditions are close to the experimentally measured results. Fig. 7b shows the layout of the three-dimensional numerical model with the structure in position. The structure was rotated by an angle of 30° corresponding to $\beta = 30°$. The slopes were smooth.

2.2.2.4. Mesh. For the empty 3D numerical wave basin, the mesh was orthogonal and conformal. It presents 3 zones in x direction with variable cell size. On the first zone from $x = 0$ m to $x = 9$ m, the grid size Δx decreased linearly from 0.07 m to 0.046 m. On the second zone ($x = 9$ m to 16.5 m), the grid size Δx was constant and equalled to 0.046 m. On the third zone ($x = 16.5$ m to 23 m), the grid size Δx grew linearly to 0.06 m. The grid size Δy in y direction near the initial free surface level was constant at 0.037 m and gradually increased to 0.046 m near the bottom and near the atmosphere boundary. In z direction, the grid size Δz was constant which was equal to 0.1 m. The mesh of the numerical basin with a structure was somewhat different from the mesh of the empty numerical basin. The base mesh without the structure was not strictly orthogonal. Instead, it gradually became oblique from the inlet boundary to the structure such that the grids near the structure were parallel with the slope surface of the dikes. The grid size Δx was constant and equal to 0.046 m in the region where the dike was located. The grid size in y direction was the same as that of the empty numerical wave basin. In z direction, the grid size Δz in the range of $z = 7$ m to 9 m is constant and equalled to 0.05 m and increased linearly up to 0.12 m at the side walls. The reason for the finer mesh in the range of $z = 7$ m to 9 m is explained later in Section 2.2.2.2. The structure was removed using snappyHexMesh with one level of refinement around the structure. The mesh generated in this way was more regular and more computationally efficient than the mesh created by removing the structure from the orthogonal and conformal base mesh. Overall, the 3D mesh was relatively coarse compared with the above 2D numerical mesh.

2.2.2.5. Wave generation. The irregular waves were generated using the relaxation zone technique implemented in waves2Foam (as introduced in Section 2.1.2.2) based on the JONSWAP spectrum using the first-order irregular wave theory that is a simple linear superposition of first order Stokes waves. The generated wave signal was not the same as that from the experiments since the original steering file from the

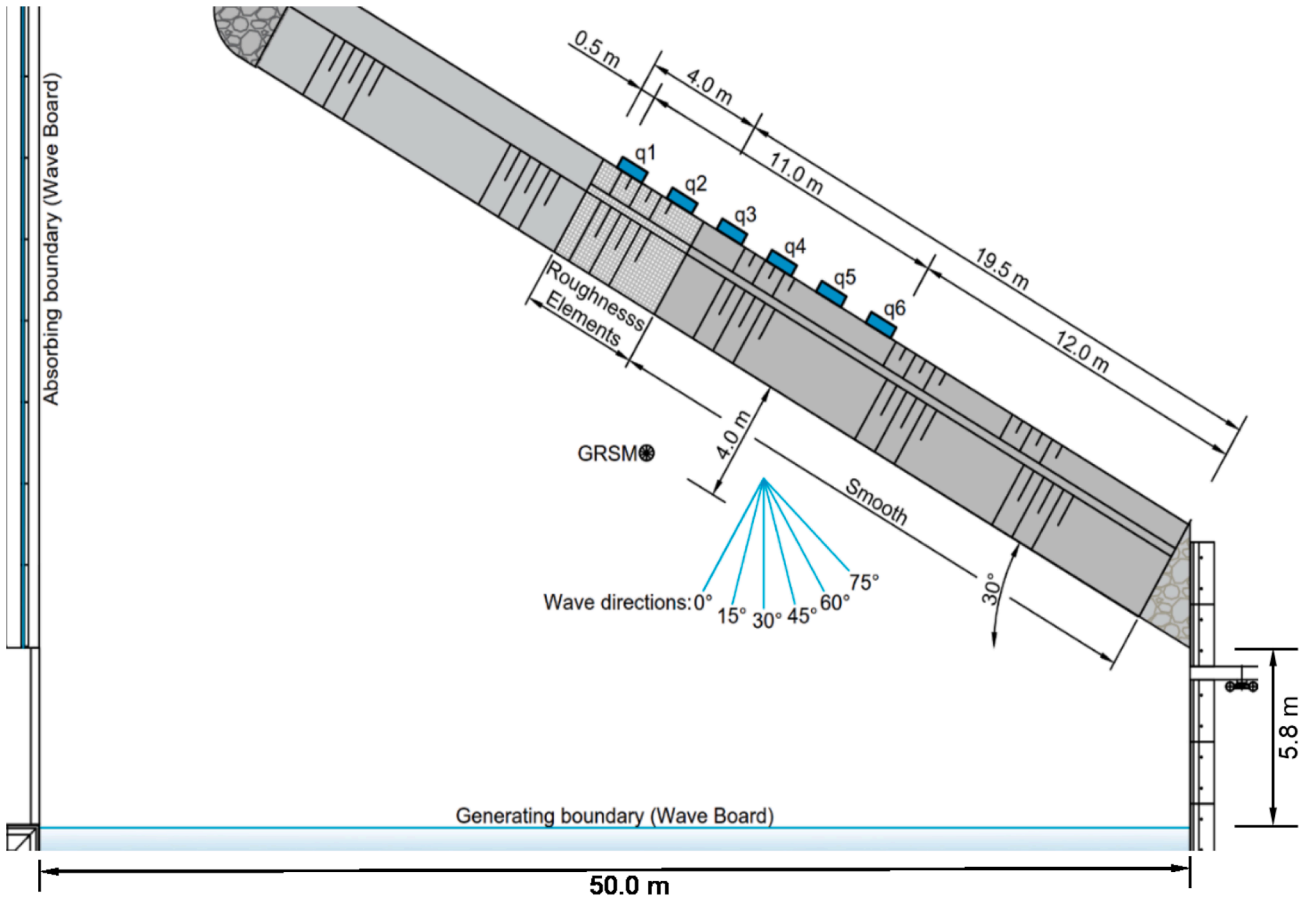

a)

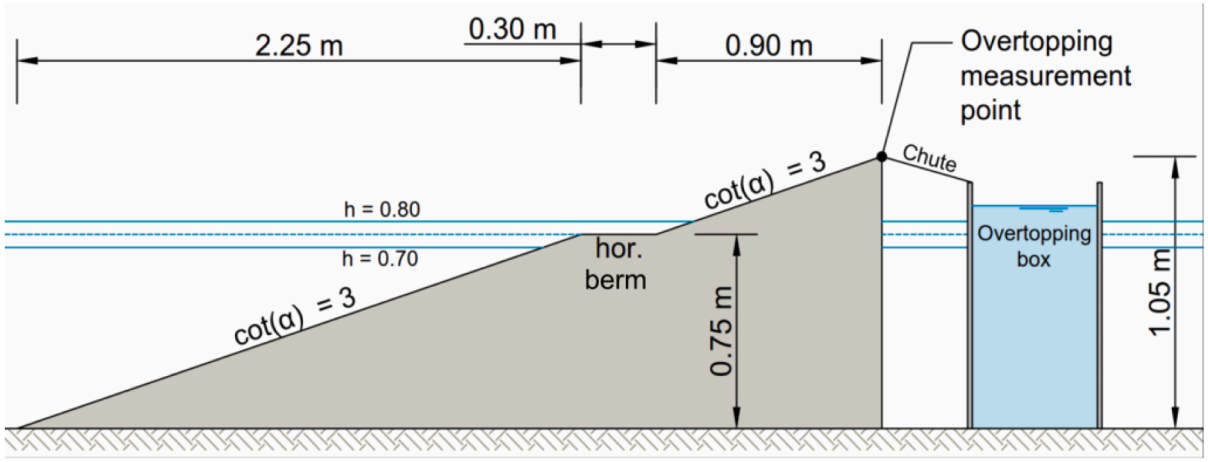

b)

Fig. 6. Three-dimensional physical model set-up with a) layout of the model in the wave basin and b) tested cross-section (from Van Gent, 2020). .

experiments was not available, but had similar wave properties as the experiments. Two relaxation zones were applied at the side walls to absorb reflected waves from the structure. The width of each side wall relaxation zone was 2 m. The simulated wave condition was first calibrated in an empty numerical wave basin without the structure in position as shown in Fig. 7a to ensure the numerically generated wave properties were close to the experimental ones. The calibrated wave condition was applied later to the numerical model with the structure in position. One set of wave gauges (WG_loc10 and WG_loc10') were defined at the start of the basin in both empty numerical model and the model including the structure, in order to check the efficiency of the side wall relaxation zone in absorbing the reflected waves from the structure by comparing the incident waves predicted by the models with and without the structure.

The 3D simulation period was set at 200 s, which took three weeks to compute parallelizing the case into 22 processors (2.7 GHz). Therefore,

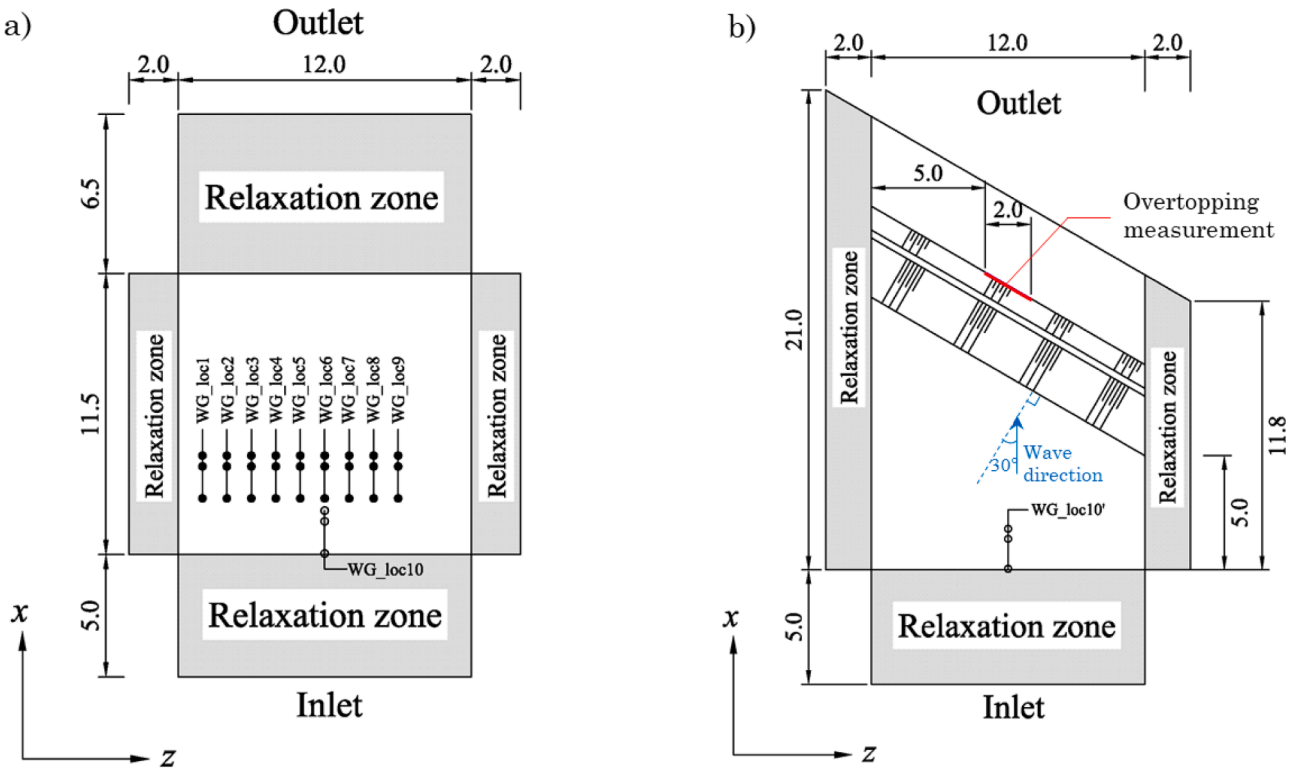

Fig. 7. Layout of a) the numerical wave basin without the structure in position and b) the numerical wave basin with the structure in position.

Table 3
Modelled wave properties H_{m0} and $T_{m-1,0}$ in an empty 3D numerical basin (the experimental wave properties are: $H_{m0} = 0.199$ m, $T_{m-1,0} = 2.57$ s and $s_{m-1,0} = 0.019$). .

	x [m]	z [m]	H_{m0} [m]	$T_{m-1,0}$ [s]	$s_{m-1,0}$ [-]
WG_loc1	7.3, 8.61, 9.05	3	0.127	2.43	0.014
WG_loc2		4	0.158	2.46	0.017
WG_loc3		5	0.180	2.51	0.018
WG_loc4		6	0.192	2.57	0.019
WG_loc5		7	0.198	2.65	0.018
WG_loc6		8	0.199	2.67	0.018
WG_loc7		9	0.198	2.65	0.018
WG_loc8		10	0.192	2.57	0.019
WG_loc9		11	0.180	2.51	0.018

considering the 3D numerical modelling was extremely time-consuming, only one 200 s numerical simulation ($H_{m0} = 0.199$ m, $T_{m-1,0} = 2.57$ s, $h = 0.8$ m and $\beta = 30°$) was performed for the validation of the 3D numerical model. Since the application of side wall relaxation zones would affect the incident waves along the z direction especially near the side relaxation zones, the waves along the z direction were not entirely uniform. The range ($z = 7$ m to 9 m) in which the wave properties were nearly uniform was determined using nine sets of wave gauges (WG_loc1 to WG_loc9 in Fig. 7a) defined along the z direction (See Table 3). A set of faces along the crest edge were selected in the range of $z = 7$ m to 9 m as shown in Fig. 7b to extract the overtopping flux using the approach given by Jacobsen (2017) based on which the mean overtopping discharge could be obtained. Thus, the grid size along the width of the basin between $z = 7$ m and 9 m was finer than the remaining region. Then, the numerically modelled overtopping discharge can be compared with the physically measured discharge to validate the 3D numerical model.

2.2.3. Numerical experiments

Van Gent (2020) proposed an empirical formula for estimating the influence of oblique waves on the mean overtopping discharge as follows:

$$\gamma_\beta = \cos^2\beta + 0.35\left(1 - \cos^2\beta\right)\left(1 + \frac{B}{H_{m0}}\right)^{-1} \tag{6}$$

Where γ_β [-] is the influence factor of oblique waves. β [°] is the angle between the direction of the waves and the perpendicular to the long axis of the dike. B [m] is the berm width. However, the berm width was fixed through the experiments, so the ratio B/H_{m0} was varied in the physical tests by varying the wave height but not by varying the berm width. Therefore, the dependency of the influence factor of oblique waves on B/H_{m0} in Eq. (6) is partly an assumption. In order to check the dependency of the oblique wave factor on berm width, 3D numerical experiments were performed on five berm widths (0 m, 0.1 m, 0.3 m, 0.4 m, 0.6 m). The TAW (2002) overtopping Eq. (7) for breaking waves was used to obtain the oblique wave factors:

$$\frac{q}{\sqrt{gH_{m0}^3}} = \frac{0.067}{\sqrt{\tan\alpha}}\xi_{m-1,0}\exp\left(C_b\frac{Rc}{H_{m0}\xi_{m-1,0}\gamma_b\gamma_f\gamma_\beta}\right) \tag{7}$$

In order to determine the values of the oblique wave factor, the berm influence factor γ_b should be determined first. One reference case with a smooth straight waterside slope and with a perpendicular incident wave direction relative to the structure was simulated in the 2DV OpenFOAM® model, which saved a lot of computational time. Overtopping discharges over different berm widths with perpendicular incident waves direction were also simulated using the 2D numerical model. A mesh resolution similar to the 3D model at $z = 6$ m (Fig. 7b) was applied in the 2D numerical model. In both 2D and 3D numerical models, the same wave condition with $H_{m0} = 0.199$ m, $T_{m-,10} = 2.57$ s and $h = 0.8$ m was imposed. The coefficient C_b in Eq. (7) was first calibrated using the 2D model results of the reference case. The berm influence factors can then be calculated by solving the Eq. (7) with $\gamma_\beta = 1$ and $\gamma_f = 1$ based on the 2D numerical data. With the coefficient C_b and berm factor γ_b known, the values of influence factor of the oblique waves can be determined using the 3D model results.

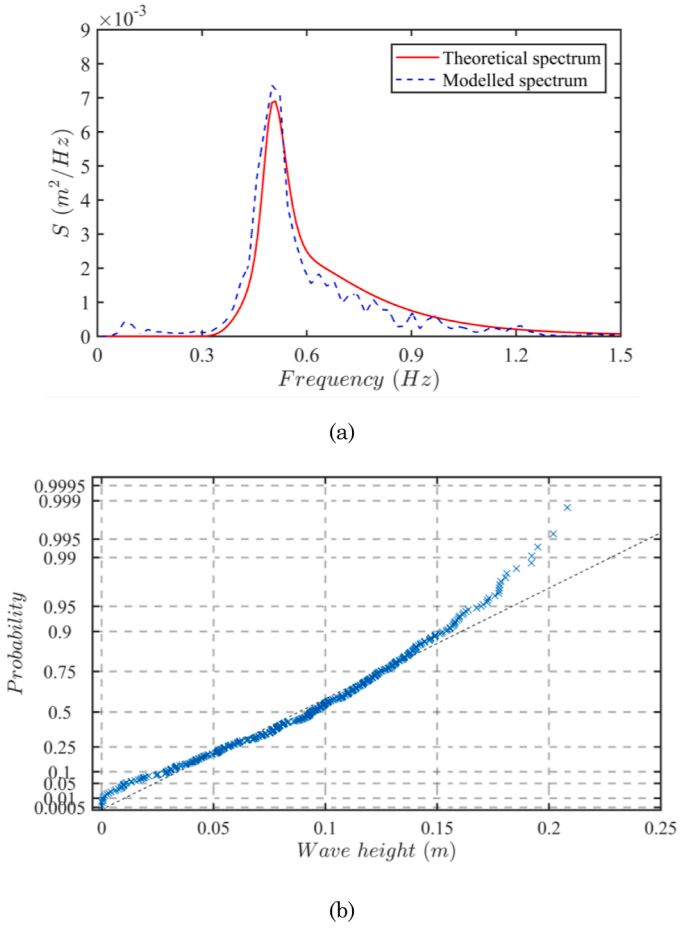

Fig. 8. Comparison between the numerically modelled (at the toe of the dike) and theoretical (a) wave spectrum of incident waves and (b) wave height distribution for test T104 (input for the theoretical wave spectrum: $H_{m0} = 0.15$ m, $T_p = 2.0$ s, $h = 0.85$ m). The black dash line in (b) represents the Rayleigh distribution.

3. Model validation

3.1. Validation of the 2D numerical model

3.1.1. Wave characteristics

Since the original measured wave spectrum and wave height distribution were not available for comparison with numerically modelled results, the theoretical results (i.e. a Rayleigh wave height distribution and a TMA wave energy spectrum) were used here. Fig. 8 shows a detailed comparison between the numerically modelled and theoretical TMA wave spectrum (Fig. 8a) and wave height distribution (Fig. 8b) for test T104. The numerical wave spectrum was determined near the toe of the dike. The input for the wave generation in the numerical model was based on the theoretical wave spectrum. Although the peak wave period is very close to the theoretical peak, the modelled incident wave spectrum shifts slightly to the left compared to the theoretical spectrum as shown in Fig. 8a. This can be caused by nonlinear wave interactions that cause some energy transfer to lower frequencies in the relatively shallow water near the toe of the structure. Fig. 8b shows that the modelled wave height distribution follows the Rayleigh distribution in general with some deviation for large wave heights. This deviation can arise from the wave breaking due to the small water depth at the toe of the structure. Overall, the modelled wave spectrum and wave height distribution match the theoretical results reasonably. Although not presented in this paper for sake of brevity, similar results were found for other cases. Numerically modelled and measured wave characteristics for all selected cases were compared as shown in Fig. 9. The numerical data for the model validation are presented in Table B.3. A good agreement can be observed from Fig. 9a between the numerical and experimental significant wave height with a mean absolute percentage error (MAPE) of 1%. However, Fig. 9b shows that the spectral wave period was overestimated by the numerical model with MAPE = 16%. Although the total amount of wave energy is computed accurately, it seems as if the wave energy is distributed too much to the lower frequencies.

In order to find a better solution for the overestimation of wave period, sensitivity analysis of the wave period $T_{m-1,0}$ of one test T104 with the grid size and length of the inlet relaxation zone was performed as presented in Fig. 10. It shows that refining the mesh or increasing the length of the inlet relaxation zone did not lead to significant improvement of the estimates of $T_{m-1,0}$. The overestimation of the wave period might be related to the wave breaking. The wave breaking could happen

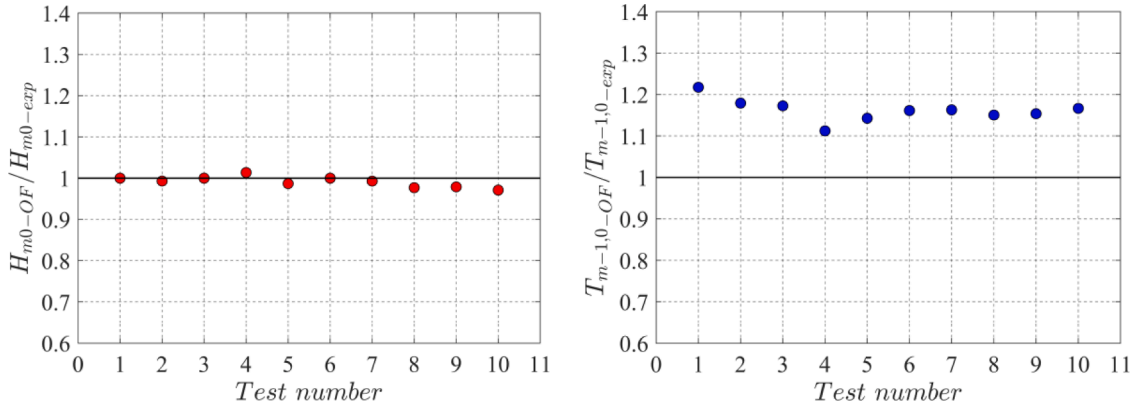

(a) Significant wave height H_{m0} (b) Spectral wave period $T_{m-1,0}$

Fig. 9. Comparison between modelled and measured wave characteristics with (a) Significant wave height H_{m0} and (b) Spectral wave period $T_{m-1,0}$.

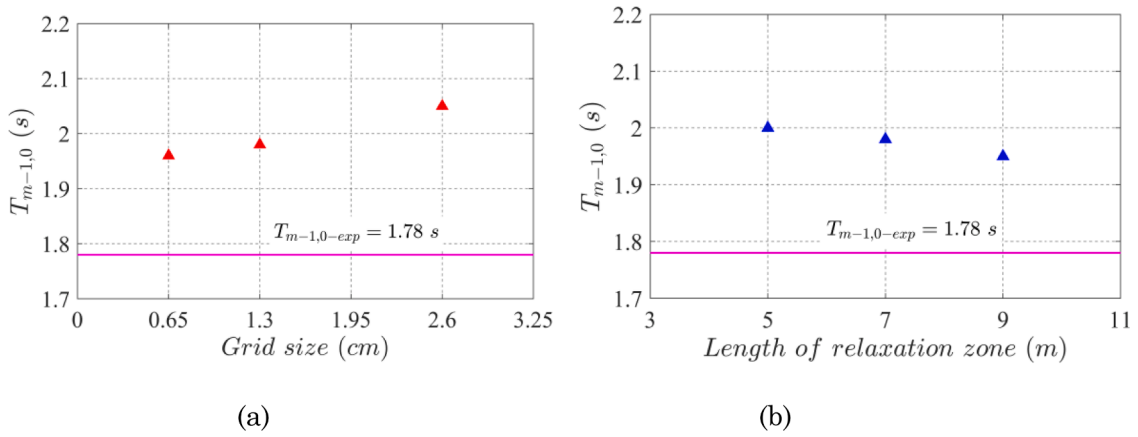

Fig. 10. Sensitivity of the numerically modelled spectral wave period $T_{m-1,0}$ (a) with the grid size: 0.65 cm × 0.65 cm, 1.3 cm × 1.3 cm, 2.6 cm × 2.6 cm (from left to right) and (b) with the length of the inlet relaxation zone: 5 m, 7 m, 9 m (from left to right). The experimentally measured $T_{m-1,0-exp}$ is 1.78 s.

due to the presence of foreshore and it cannot be dealt with very well by the OceanWave3D as the wave breaking is taken into account by using a parameterization method, which led to inaccuracies of the wave period. The spectral wave period $T_{m-1,0}$ given by OceanWave3D was 1.93 s. This overestimation of the wave period in OceanWave3D further caused the overestimation ($T_{m-1,0}$ = 1.98 s) in the OpenFOAM model. A second potential explanation of the difference may be related to the shorter computations (about 300 waves) compared to the experiments (1000 waves). Since the main focus of this study is the overtopping behaviour predicted by the numerical model, we will not further explore the solution in this paper and recommend to further investigate this issue in the future. Consequently, the overestimation of the wave period could cause an overestimation of the flow velocity and the layer thickness, which will be explained later in Section 3.1.2.

3.1.2. *Flow velocity and layer thickness*

The calculated flow velocities and layer thickness using Van Gent (2002a) Eqs. (1) & (2) were first compared with the experimental results. The wave run-up height presented in Eqs. (1) & (2) was calculated using Eq. (A. 1). The green squares in Fig. 11 represent the comparison between the measured results from experiments and calculated ones in which the experimental wave height and wave period were applied. Since the empirical equations were derived based on the extensive experimental data presented in Van Gent (2002a) and the experimental data for the model validation were just a part of the entire dataset, slight deviations between the calculated and measured results can be seen in Fig. 11. Nevertheless, there is an overall good agreement for both flow velocity and layer thickness. It is worth noting that applying the wave properties given by the numerical model to calculate the flow characteristics resulted in larger flow velocities and layer thickness (see yellow triangles). The numerical and experimental significant wave heights were almost the same as shown in Fig. 9a while the numerical wave periods were obviously larger than the experimental ones, so Fig. 11 indicates that larger wave periods led to larger values of flow characteristics.

Therefore, before directly comparing the numerically modelled flow velocities and layer thicknesses with the experimental ones, the modelled flow characteristics for each case were first modified by taking the overestimation of the spectral wave period into account using the following equation:

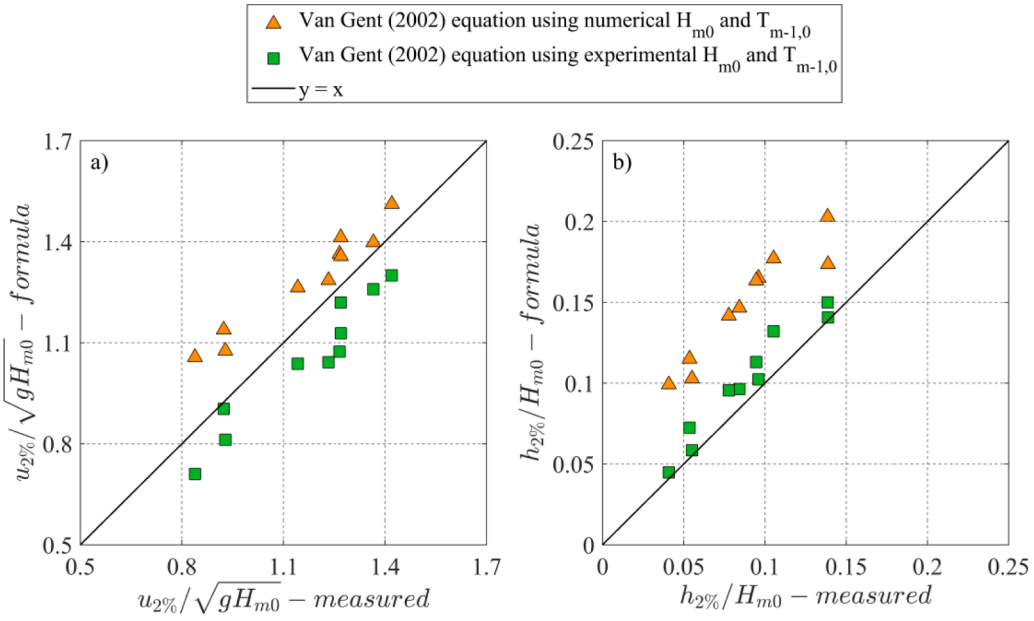

Fig. 11. Comparison between measured and estimated flow parameters with a) flow velocity and b) layer thickness exceeded by 2% of the incident waves given by empirical equations using the experimental and numerical wave characteristics. .

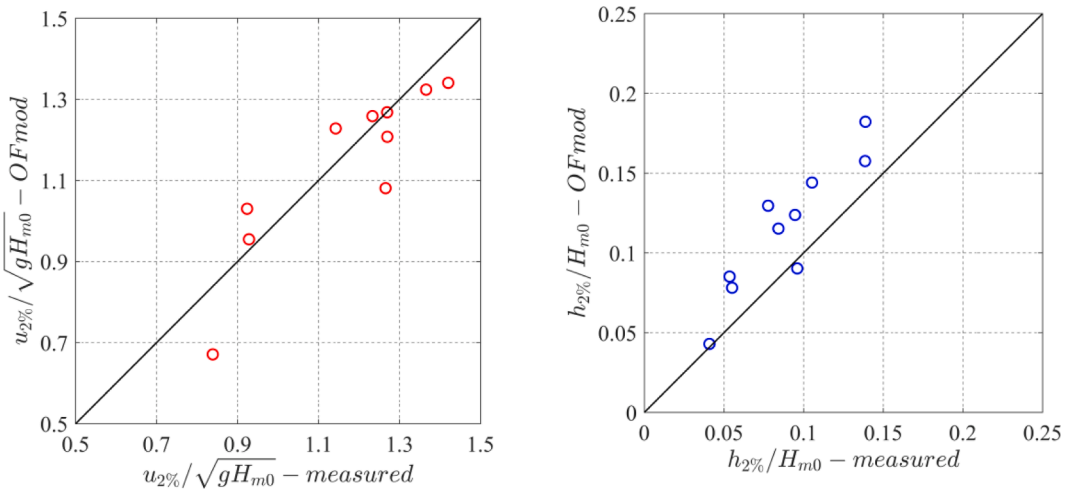

(a) Flow velocity (b) Layer thickness

Fig. 12. Comparison between the measured flow parameters and the modified flow parameters given by OpenFOAM® model taking the overestimation of the wave period into account. .

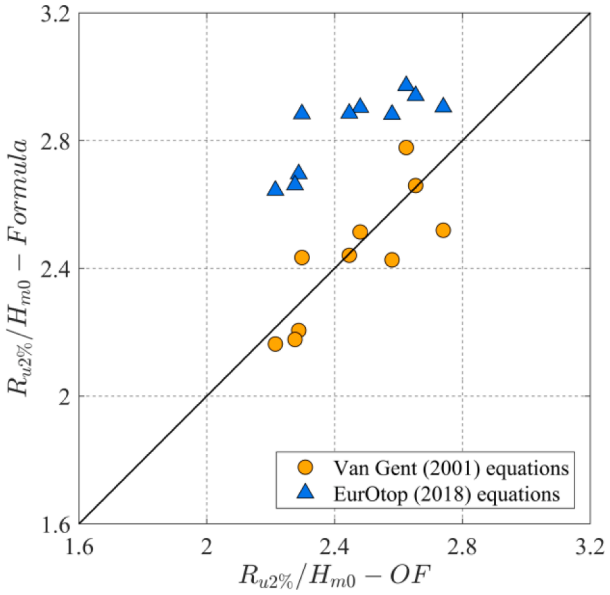

Fig. 13. Modelled and calculated wave run-up heights using Van Gent (2001) run-up equation (A.1) and EurOtop (2018) run-up equations (A.2, A.3). .

$$x_{2\%OFmod} = \frac{x_{2\%OF}}{x_{2\%cal-OF}/x_{2\%cal-exp}} \tag{8}$$

where $x_{2\%OFmod}$ [m/s] is the modified modelled flow velocity or layer thickness; $x_{2\%OF}$ is the original modelled flow parameter; $x_{2\%cal-OF}$ [m/s] is the calculated flow parameter using the empirical equations (Van Gent, 2002a) in which the numerically modelled wave characteristics were used; $x_{2\%cal-exp}$ is the calculated flow parameter using the empirical equations Van Gent (2002a) in which the experimental wave characteristics were applied.

The comparisons between the modified modelled and the measured flow characteristics are shown in Fig. 12. The modified modelled flow velocity matches well with the measured results with a NSE of 0.75. In contrast, the NSE for the modified layer thickness is 0.03. The low value of NSE is mainly caused by the overestimation of the layer thickness given by the OpenFOAM® model. On average, the numerical model overestimates the layer thickness with a factor of 1.3 and dividing the modified modelled results of the layer thickness by 1.3 can increase the NSE from 0.03 to 0.83, illustrating that the trend in the layer thickness is well captured by the numerical model. This overestimation can be related to different time series of waves used in the OpenFOAM model and the experiments. Another possible cause might be the quality of free surface capture. The interface between water and air was not very sharp and could smear out over two layers of grid cells in the numerical model, which can further result in an overestimation of the layer thickness. Similar overestimation of layer thickness by OpenFOAM® models can also be found in Van Bergeijk et al. (2020). Refining the mesh near the waterside slope and crest can to some extent reduce the overestimation. Nevertheless, a fine mesh would significantly increase the computational time especially for the slope covered by protruding blocks. Therefore, the grid size of 0.005 m in vertical direction is adopted to comprise between the computational efficiency and the model accuracy of layer thicknesses. Despite of a low value of NSE (0.03), the overestimation with a factor of 1.3 is considered as being acceptable given the spreading that is normally observed when dealing with measurements of wave overtopping parameters (see for instance Fig.9 in Mares-Nasarre et al., 2019).

Considering the wave run-up height is a key parameter for estimating the flow velocity and layer thickness (see Eqs. (1) & (2)), the modelled wave run-up heights were compared to the empirical equations (A.1 and A.2) as the wave run-up height was not measured in the experiments from Van Gent (2001). Fig. 13 shows that the model results match well with the Van Gent (2001) run-up equation (A.1) with a NSE of 0.56 while the EurOtop (2018) equations (A.2 & A.3) overestimate the wave run-up height with a factor of 1.2 and with a NSE of −3.9. The difference between Van Gent (2001) and EurOtop (2018) run-up equations mainly lies around the transition between breaking and non-breaking wave conditions; most of the data in this study are close to this transition between breaking and non-breaking waves. A smooth transition at a certain value of the Iribarren parameter $\xi_{m-1,0}$ was proposed by Van Gent (2001) considering the derivative with respect to $\xi_{m-1,0}$ of Eq. (A.1) should be continuous in a physical sense. EurOtop (2018) proposed an abrupt transition near the transition between breaking and non-breaking wave conditions based on the analysis of extensive datasets. Fig. 13 indicates that the model results match better with Van Gent (2001) run-up equation (A.1) than with the EurOtop (2018) equations (A.2, A.3).

Since this study focuses on the predictions of flow parameters and the influence of berms and roughness on these flow parameters (instead of on the accuracy of the incident wave characteristics), the numerical

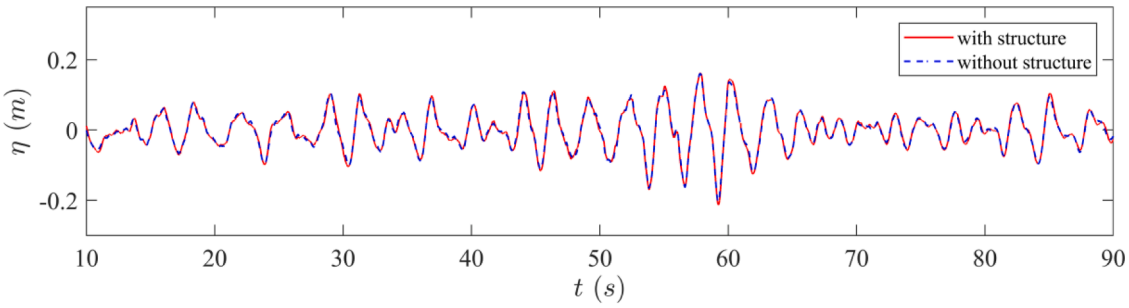

a) Time series of incident free surface elevation

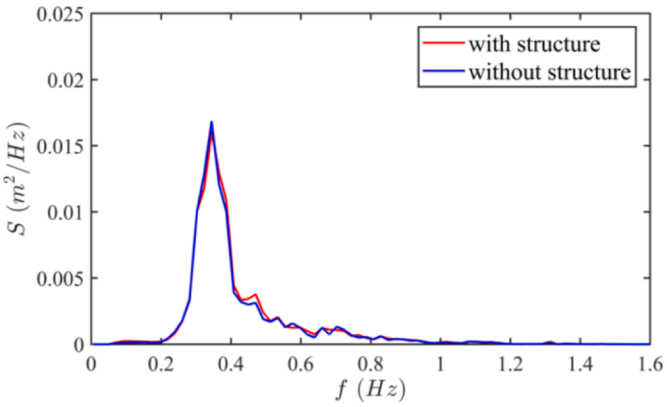

b) Wave energy spectrum of incident waves

Fig. 14. Comparison of incident waves between the numerical wave basins with and without the structure.

Table 4
Wave properties near the inlet in the numerical wave basins with and without structure.

	H_{m0} [m]	$T_{m-1,0}$ [s]	$s_{m-1,0}$ [-]
With structure	0.19	2.65	0.017
Without structure	0.187	2.65	0.017

Table 5
Measured and modelled wave characteristics and average overtopping rates.

	Experiment	OpenFOAM®
H_{m0} [m]	0.199	0.198
$T_{m-1,0}$ [s]	2.57	2.66
$s_{m-1,0}$ [-]	0.019	0.018
q [l/s/m]	0.65	1.9

model is regarded as being capable of predicting the flow velocities and layer thickness sufficiently accurate.

3.2. Validation of the 3D numerical model

3.2.1. Wave characteristics

The incident waves at the start (WG_loc10 and WG_loc10') of the 3D numerical wave basin with and without the structure were compared as shown in Fig. 14. A good agreement on both the time series of incident waves and the wave energy spectrum between the model with structure and the model without structure can be seen in Fig. 14, which indicates that there was little wave reflection at the side walls interfering the incident waves. Table 4 presents the wave properties measured by the wave gauges near the inlet in the numerical basins with and without the structure. The incident wave height at the inlet of the basin is slightly larger compared with the wave height in an empty wave basin. Nevertheless, the difference is small, which is acceptable.

3.2.2. Mean overtopping discharge

The overtopping flux was extracted in the range of $z = 7$ m to 9 m where the waves were nearly uniform along the z axis. The measured and modelled wave conditions and overtopping discharges are given in Table 5. The modelled average overtopping discharge is 1.9 l/s/m which is about three times of the measured overtopping rate ($q_{exp} = 0.65$ l/s/m). One of the causes for this overestimation might be the short simulation time (200 s) which could lead to more uncertainties than a long simulation time (e.g. 1000 waves) of the estimation of overtopping rates. However, EurOtop (2018) stated that empirical equations estimated overtopping discharges at best within a factor of 1 to 3 of the actual overtopping discharges. Therefore, this overestimation with a factor of 3 is reasonable (see for instance Suzuki et al., 2017). The trend of the overtopping discharge due to oblique waves changing with the berm width is more of interest in this study than the absolute values of the overtopping discharge themselves. This means that the 3D numerical model is used in a qualitative way. Hence, although only one test condition was simulated for the 3D model validation, this model validation is regarded as being acceptable in this study. The wave conditions and numerical model settings for this validation test are later enforced for other 3D simulations in which only the berm width is different to find the trend of the influence factor of oblique waves varying with the berm width.

4. Effects of roughness, a berm and oblique waves on overtopping parameters

The validated OpenFOAM® models were then applied to investigate

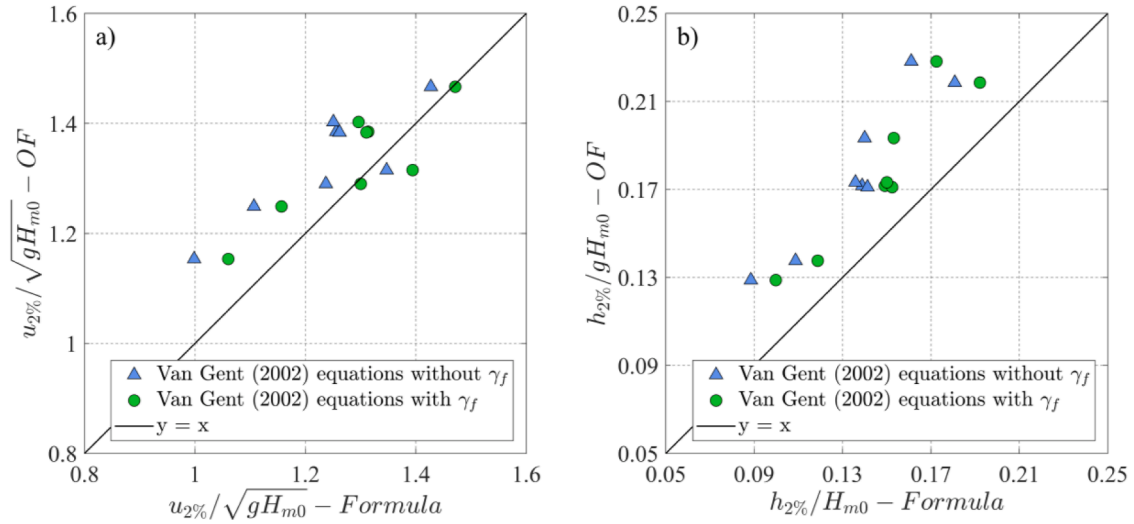

Fig. 15. Comparison between numerically modelled a) flow velocities as well as b) layer thickness and the calculated ones over the rough slope using the Van Gent (2002a) Eqs. (1) & (2) with and without including the roughness factor γ_f.

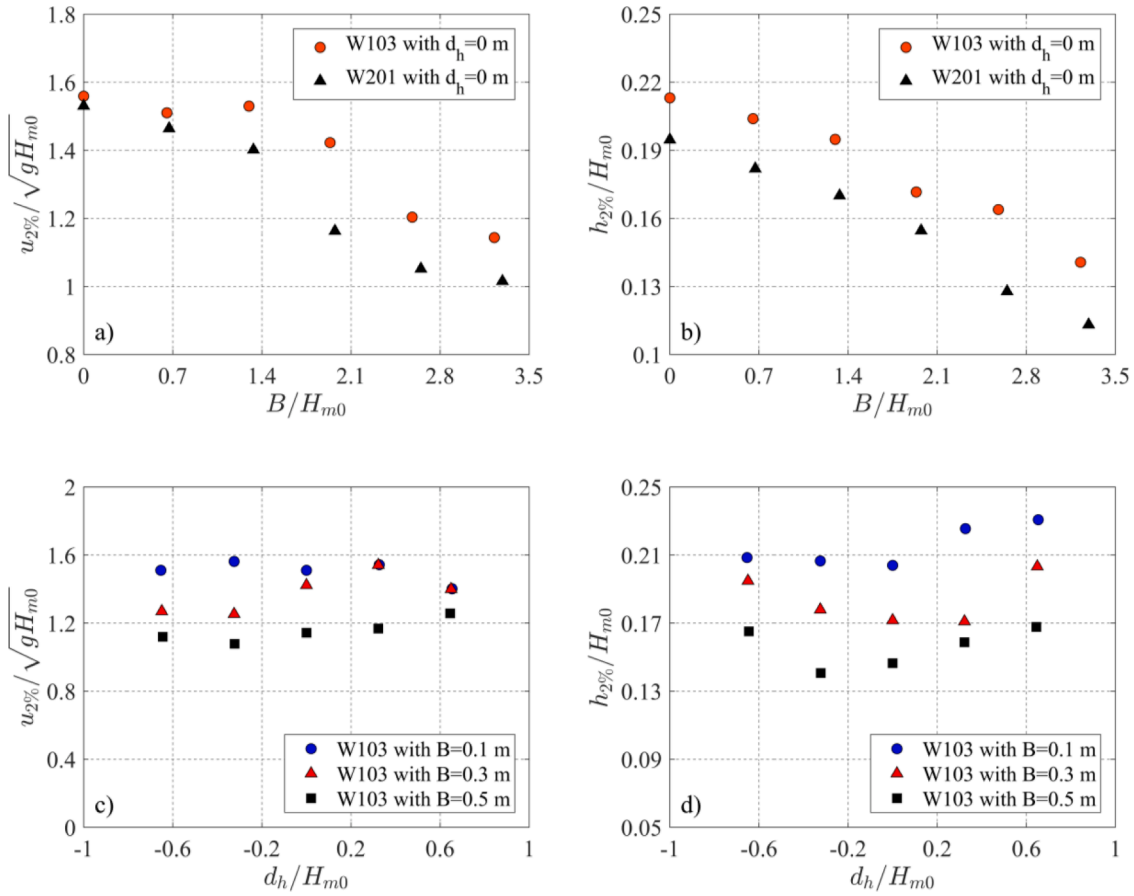

Fig. 16. The influence of berm width (B) and berm level (d_h) on the extreme overtopping flow velocity $u_{2\%}$ and layer thickness $h_{2\%}$ with W103 representing the wave condition based on single-peaked TMA spectrum: $H_{m0} = 0.152$ m, $T_{m-1,0} = 2.51$ s, $h = 0.8$ m and W201 representing the wave condition based on double-peaked TMA spectrum: $H_{m0} = 0.149$ m, $T_{m-1,0} = 2.32$ s, $h = 0.8$ m.

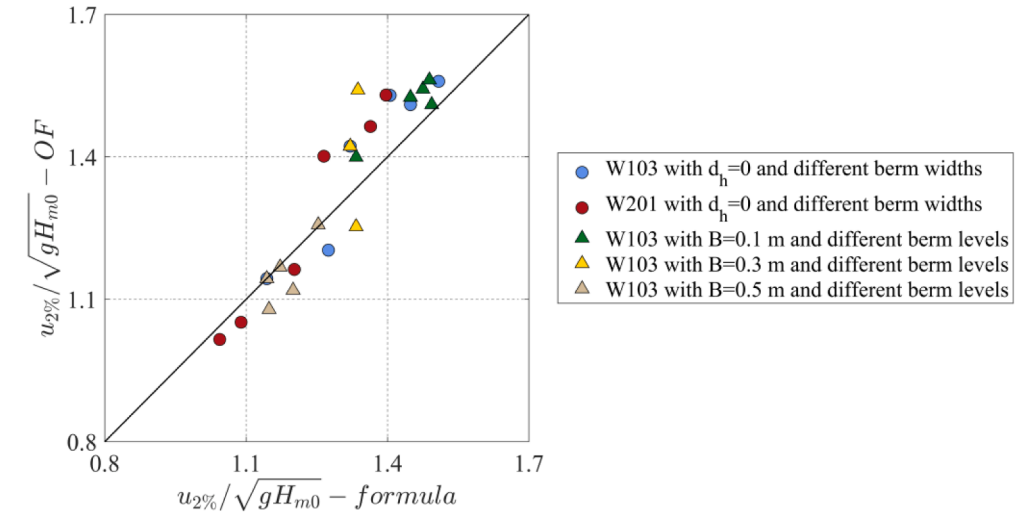

(a) Flow velocity

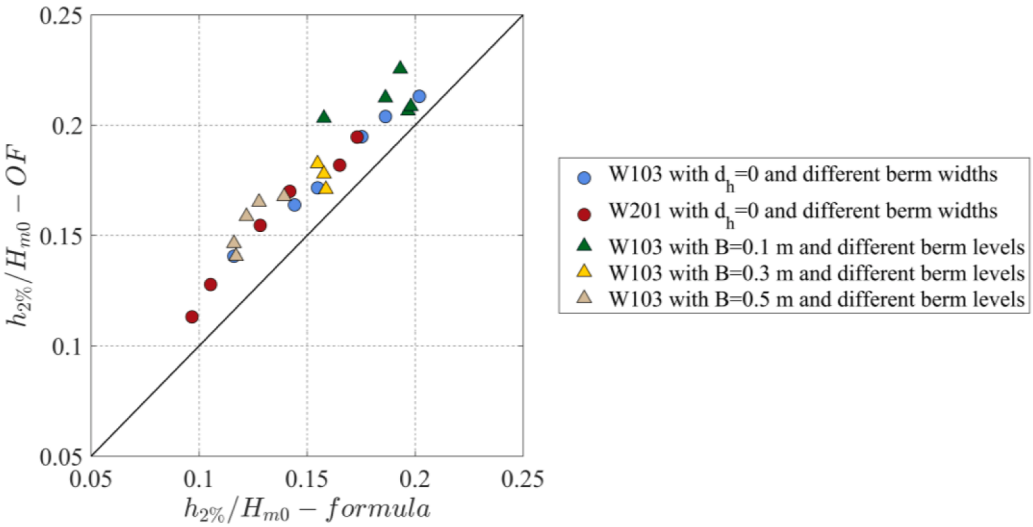

(b) Layer thickness

Fig. 17. Comparison between the modelled flow parameters and the calculated values using modelled wave run-up heights by empirical equations with the berm width varying in the range of 0 m to 0.5 m and the berm level in the range of −0.1~0.1 m. W103 represents the wave condition based on single-peaked TMA spectrum: $H_{m0} = 0.152$ m, $T_{m-1,0} = 2.51$ s, $h = 0.8$ m and W201 represents the wave condition based on double-peaked TMA spectrum: $H_{m0} = 0.149$ m, $T_{m-1,0} = 2.32$ s, $h = 0.8$ m.

the effects of roughness, berm and oblique waves on flow parameters and overtopping discharges. In this section, the results of both 2D and 3D numerical experiments were analysed.

4.1. *The influence of roughness on flow parameters*

According to the literature review, it still remains unclear whether to include the roughness reduction factor in Eqs. (1) & (2). To figure this out, the roughness was modelled in the 2DV numerical model by creating protrusions along the waterside slope. The modelled flow characteristics were compared with the calculated ones using empirical equations with and without the roughness influence factor. The values of roughness factor were obtained by comparing the wave run-up height at the rough slopes with that at the smooth slope. Since the 2DV numerical model was validated based on the experimental results in Van Gent (2002a), only the Van Gent (2002a) equations for flow characteristics including and excluding the roughness factor were considered here.

Fig. 15 shows the comparison between modelled and calculated flow characteristics using the Van Gent (2002a) equations with and without the roughness influence factor. For calculations of flow velocities and layer thicknesses, the modelled wave run-up heights at the rough slope were used instead of using the empirical equation (A.1) for the wave run-up height. It can be observed in Fig. 15 that excluding the roughness factor in Eqs. (1) & (2) leads to underestimation of flow characteristics. Including the roughness factor leads to better estimates of flow velocities improving the NSE from −0.5 to 0.35. However, including the roughness factor still underestimates the layer thicknesses with a factor of 0.84 of the numerically modelled layer thickness. Nevertheless, it can reduce the underestimation to some extent, considering that excluding the roughness factor results in a factor of 0.77. This underestimation of the layer thickness could partly be caused by the slight overestimation of layer thicknesses given by the OpenFOAM® model as shown in Fig. 12b.

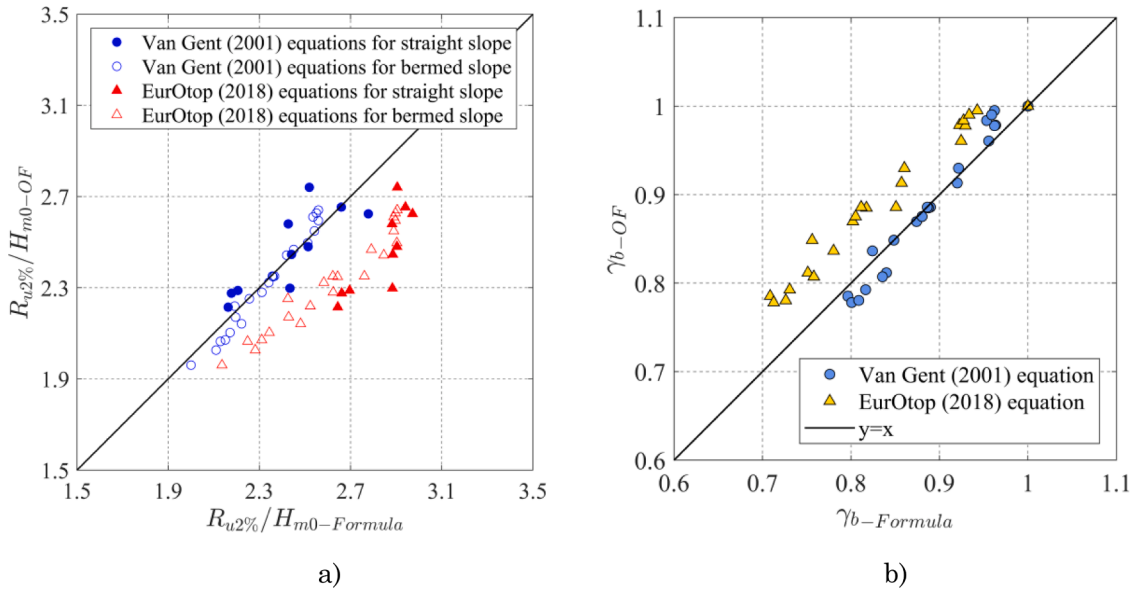

Fig. 18. Comparisons between a) modelled and calculated wave run-up heights over straight and bermed slopes using Van Gent (2001) equations and EurOtop (2018) equations; b) modelled and calculated berm influence factors using empirical equations proposed by Van Gent (2001) and EurOtop (2018).

For the smooth straight slope, the numerically modelled layer thicknesses are about 1.16 times of the estimated ones using the empirical equations. Dividing the OpenFOAM® modelled layer thicknesses by 1.16 and including the roughness factor in Eq. (2) finally lead to estimates of layer thicknesses with a factor of 0.97 of the numerically modelled ones and a NSE of 0.85. These results indicate that it is indeed better to include the roughness factor in Eqs. (1) & (2) as proposed. The roughness factor in this study only varied in the narrow range of 0.88 to 0.95. Therefore, the difference between including and excluding the roughness factor in Eqs. (1) & (2) for smaller values of the roughness factor can be larger. Empirical equations similar to Eqs. (1) & (2) but excluding the roughness factor could lead to estimates of flow characteristics that are too low and thus unsafe.

4.2. The influence of a berm on flow parameters at the waterside edge of the crest

In order to study the berm influence, the berm width was varied in the range of 0 m to 0.5 m and berm level relative to SWL was changed in the range of −0.1 m to 0.1 m by changing the berm position. Fig. 16 shows the influence of berm width and berm level on the flow velocity and layer thickness. It can be seen that the flow parameters are sensitive to the variations in the berm width. The flow velocity and the layer thickness could be reduced by nearly 30% and 40% respectively due to the application of a berm. In contrast, the berm level did not have a significant reductive effect on the flow characteristics.

The modelled flow characteristics at smooth slopes with a berm were first compared to the Van Gent (2002a) empirical formulas Eqs. (1) & ((2)). In order to calculate the flow parameters using Eqs. ((1) & (2)), the wave run-up height needs to be known. It is worth mentioning that the flow parameters on the horizontal axis in Fig. 17 were calculated using the numerically modelled wave run-up heights instead of using the empirical run-up equation (A. 1). Fig. 17 shows that the calculated flow velocities match well with the OpenFOAM® model results with a *NSE* of 0.79. The calculated values of the layer thickness are generally smaller than the modelled results leading to *NSE* = 0.24. This is caused by the slight overestimation of the layer thickness given by the OpenFOAM® model as presented in Fig. 12b. Overall, the numerical results demonstrate that the relationships between the flow parameters and the wave run-up height as given in Van Gent (2002a) equations ((1) & (2)) are also valid for smooth slopes with a berm, which implies that the berm influence is accounted for by the wave run-up height. Thus, the investigation of the berm effect on flow characteristics comes down to the investigation of the influence of a berm on the wave run-up height.

Fig. 18a shows the comparison between the modelled run-up heights at straight slope as well as slopes with a berm and the calculated ones using Van Gent (2001) equation (A. 1) and EurOtop (2018) equations (A. 2) & (A. 3). The berm factor γ_b, which represents the reductive influence of a berm on overtopping discharge or run-up height, in EurOtop (2018) equations (A. 2) & (A. 3) was determined using the empirical equation (A. 4). In the Van Gent (2001) equation, the berm effect was taken into account by

Table 6
Numerical results of 3D OpenFOAM® model for different berm widths with the wave direction relative to the structure $\beta = 30°$.

case	B [m]	H_{m0} [m]	$T_{m-1,0}$ [s]	$s_{m-1,0}$ [-]	q [l/s/m]
B00	0	0.198	2.66	0.018	3.1
B10	0.1	0.198	2.66	0.018	2.5
B30	0.3	0.198	2.66	0.018	1.9
B40	0.4	0.198	2.66	0.018	1.6
B60	0.6	0.198	2.66	0.018	1.2

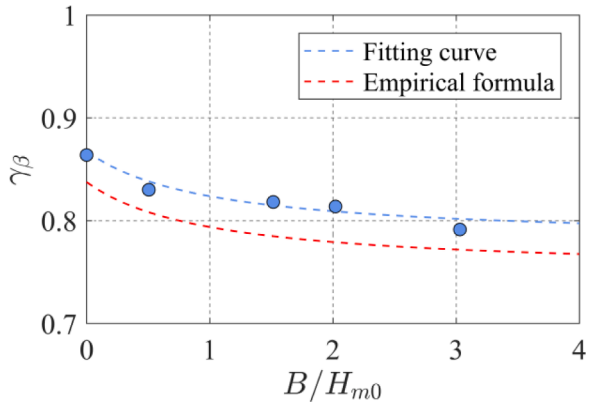

Fig. 19. Relationship between the influence factor of oblique waves with $\beta = 30°$ and the relative berm width with the red dash line denoting the empirical formula (Eq. (6)) proposed by Van Gent (2020) (For interpretation of the references to color in this figure legend, the reader is referred to the web version of this article).

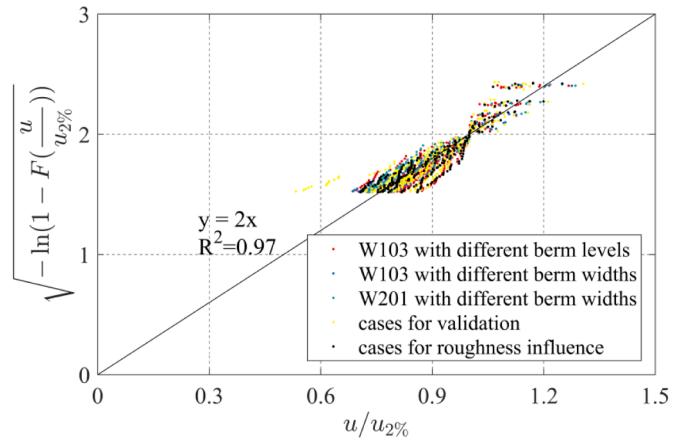

(a) Flow velocity

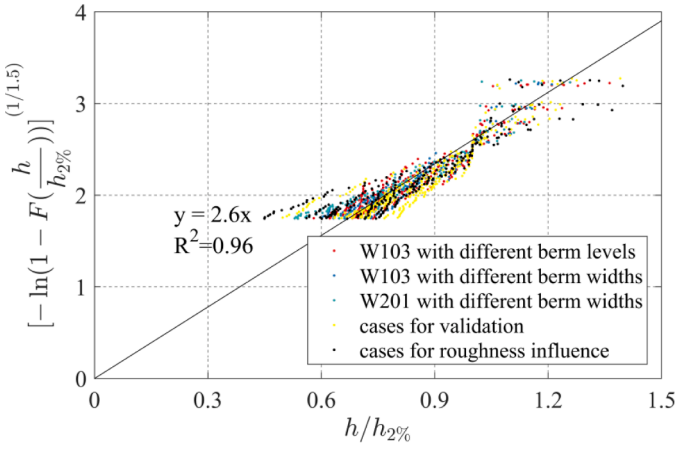

(b) Layer thickness

Fig. 20. Fitted cumulative distribution function of (a) flow velocity and (b) layer thickness in equivalent probability plot. W103 represents the wave condition based on single-peaked TMA spectrum: $\boldsymbol{H_{m0}} = 0.152$ m, $\boldsymbol{T_{m-1,0}} = 2.51$ s, $\boldsymbol{h} = 0.8$ m and W201 represents the wave condition based on double-peaked TMA spectrum: $\boldsymbol{H_{m0}} = 0.149$ m, $\boldsymbol{T_{m-1,0}} = 2.32$ s, $\boldsymbol{h} = 0.8$ m.

adopting a characteristic slope to be used in the breaker parameter. Thus, no additional reduction factor for berms is required. The characteristic slope was defined as $\tan\varphi = 2c_{BERM}H_{m0}/L$ where c_{BERM} was set at 2. Fig. 18a shows that the calculated wave run-up heights using Van Gent (2001) equation (A. 1) match very well with the modelled values while EurOtop (2018) equations (A. 2), (A. 3) & (A. 4) overestimate the wave run-up heights. Solid marks in Fig. 18a denote the data of cases for model validation. Fig. 18b shows the comparison between the berm factors obtained based on the OpenFOAM® model results and those determined using empirical equations. EurOtop (2018) berm equation (A. 4) underestimate the berm factors, which means that the equations overestimate the reductive influence of a berm on wave run-up heights. Since no berm factor was used in Van Gent (2001) run-up equation (A. 1), the berm effects were determined by comparing the calculated run-up heights taking the berm into account to those without considering the berm using the equation (A. 1). There is a good agreement between the calculated berm factors applying Van Gent (2001) approach and the numerically modelled ones with NSE = 0.94. Therefore, it could be concluded based on the model results that the existing empirical formulas proposed by Van Gent, 2001, 2002a for flow characteristics and run-up heights are also applicable for slopes with a berm.

4.3. The influence of oblique waves on the overtopping discharge

The above 2DV numerical model was extended into the 3D model domain, considering the oblique waves in combination with the berm influence. The berm influence was determined by comparing the overtopping discharge at slopes with a berm to that at a straight slope using a 2DV numerical model. Based on that, the oblique wave factors could be determined using the method described in Section 2.2.2. Results of the 3D OpenFOAM® models are given in Table 6. Fig. 19 shows that the influence factor of oblique waves overall decreases as the relative berm width increases, which indicates the influence of oblique waves on the overtopping discharge is dependant on the berm width. The blue dash line in Fig. 19 represents the fitting curve of the numerical data. Even though the absolute values of the oblique wave factor based on the OpenFOAM® model results somewhat deviate from the empirical formula (Eq. (6)) with a vertical shift of 0.023, the trend is in accordance with the trend of the relationship between the influence of oblique waves and berm width as indicated by Eq. (6). The 3D numerical model results verified the dependency of the effect of oblique waves on the berm width.

5. Discussion

5.1. Distribution functions for flow parameters

Extreme overtopping events are important to assess the safety of dikes. The distributions of extreme overtopping parameters also provide valuable information, apart from 2%-values of the flow parameters for predicting the cover erosion, which are discussed in this section. Hughes et al. (2012) suggested Rayleigh distributions for the upper 10% of the values of flow velocity and flow thickness. The 10% of the values was used since the extreme values were more relevant to the stability of coastal structures and the entire rank-ordered values led to more scatter. However, Mares-Nasarre et al. (2019) proposed an exponential distribution function for values of the flow layer thickness associated with exceedance probabilities under 2% and a Rayleigh distribution function for flow velocities with exceedance probabilities under 2%. Hence, we also analysed the distribution functions of the extreme flow parameters with exceedance probabilities below 10% based on the 2D numerical model results as suggested by Hughes et al. (2012). Flow parameters from each numerical test were rank-ordered and the Weibull distribution suggested by Hughes et al. (2012) were fit to the upper 10% of the values to determine the distribution functions for the overtopping flow velocity and layer thickness.

The Weibull distribution functions for flow velocity and layer thickness are given as below:

$$\boldsymbol{F}\left(\frac{\boldsymbol{u}}{\boldsymbol{u}_{2\%}}\right) = 1 - \exp\left[-\left(\boldsymbol{a}_1\frac{\boldsymbol{u}}{\boldsymbol{u}_{2\%}}\right)^{\boldsymbol{b}_1}\right] \tag{9}$$

$$\boldsymbol{F}\left(\frac{\boldsymbol{h}}{\boldsymbol{h}_{2\%}}\right) = 1 - \exp\left[-\left(\boldsymbol{a}_2\frac{\boldsymbol{h}}{\boldsymbol{h}_{2\%}}\right)^{\boldsymbol{b}_2}\right] \tag{10}$$

in which F represents the probability that an incident wave will lead to a flow parameter smaller than a specified flow parameter. u and h are the flow velocity and layer thickness respectively, with an exceedance probability under 10%; $u_{2\%}$ and $h_{2\%}$ were used to make u and h dimensionless as recommended by Mares-Nasarre et al. (2019); a_1 and a_2 are empirical coefficients to be calibrated; b_1 and b_2 are shape factors to be calibrated. The shape factor equal to 1 corresponds to an exponential distribution and equal to 2 corresponds to a Rayleigh distribution. The peak values of flow velocity and layer thickness were ranked in descending order for each numerical test, based on which the upper 10% (about 300 × 10%) values were selected. The a_1 and b_1 were calibrated based on the selected values for each numerical test applying the least square method. Eqs. (9) & (10) are applied on the number of incident waves in a storm. Thus, the exceedance probability corresponding to each value of the flow velocity was

calculated as k/N where k is the rank of the flow velocity value and N is the number of incoming waves. 41 cases in total were simulated using the 2D numerical model, which yielded 41 sets of a_1 and b_1. The optimal values of a_1 and b_1 were determined as the median of the 41 values. The same method was applied to layer thickness and the optimal values of a_2 and b_2 can also be obtained.

Fig. 20 shows the fitted cumulative distribution functions with R^2=0.97 for the flow velocity and $R^2 = 0.96$ for the layer thickness. The calibrated distribution functions for flow velocity and layer thickness with exceedance probabilities under 10% are presented as:

$$F\left(\frac{u}{u_{2\%}}\right) = 1 - \exp\left[-\left(2\frac{u}{u_{2\%}}\right)^2\right] \tag{11}$$

$$F\left(\frac{h}{h_{2\%}}\right) = 1 - \exp\left[-\left(2.6\frac{h}{h_{2\%}}\right)^{1.5}\right] \tag{12}$$

The distribution of the flow velocity with $b_1 = 2$ implies a Rayleigh distribution function, which is in accordance with previous research (Hughes et al., 2012; Mares-Nasarre et al., 2019). However, the distribution of layer thickness with $b_2 = 1.5$ does not correspond to a Rayleigh distribution suggested by Hughes et al. (2012) nor an exponential distribution proposed by Mares-Nasarre et al. (2019). Only seven cases were considered in Hughes et al. (2012), which could lead to many uncertainties about the results. Mares-Nasarre et al. (2019) suggested that if the flow velocity followed a Rayleigh distribution function, the layer thickness would be expected to follow an exponential distribution considering the 1/2-power relationship between the flow velocity and layer thickness exceeded by 2% of the incoming waves as shown in Eq. (13). However, the empirical coefficient C in Eq. (13) can be different for a different exceedance percentage than 2%. Thus, the layer thickness does not necessarily follow an exponential distribution function. Fig.11 in Mares-Nasarre et al. (2019) also indicates that the layer thickness did not follow the exponential distribution function perfectly. The difference between the distribution functions of the layer thickness in this study and in Mares-Nasarre et al. (2019) could also be caused by different exceedance probabilities (10% in this study and 2% in Mares-Nasarre et al., 2019) being used for deriving the cumulative distribution functions.

$$u_{2\%} = C\sqrt{g h_{2\%}} \tag{13}$$

5.2. Application and limitation of the 2D and 3D numerical models

The 2DV OpenFOAM® model showed a reasonable agreement with the measured flow velocities and layer thickness. The validated 2D numerical model was then applied to investigate the influence of roughness and a berm on flow velocity and layer thickness. The roughness was modelled by creating protrusions along the waterside slope. Model results indicate that the roughness reduction factor should be included in empirical Eqs. (1) & (2) even though the wave run-up height already takes the roughness influence into account. The existing formulas excluding the roughness factor could underestimate the flow characteristics over rough slopes. Since the flow velocity is a key input parameter in some erosion models (e.g., Dean et al., 2010), underestimation of the flow velocity might lead to underestimation of the cover erosion. This would be dangerous for reliability evaluation of coastal structures. Only one type of roughness element was modelled since this study aims to determine whether the roughness reduction factor should, or should not, be included in Eqs. (1) & (2). It is recommended to investigate the effects of different types of roughness elements with a wider range of roughness factor on the flow characteristics through physical or numerical experiments.

For the berm influence on the flow characteristics, model results demonstrate that the existing empirical Eqs. (1) & (2) proposed by Van Gent (2002a) were also applicable for the bermed slope. The berm influence on the flow characteristics was accounted for by the wave run-up height, which is different from the roughness influence that needed to be included in Eqs. (1) & (2) even though the wave run-up height had included the roughness effect. Model results of the berm infuence factor showed a good agreement with the exiting empirical equation (A.1). The effect of a berm was further analysed in combination with the oblique waves for the average overtopping discharge. The 2D numerical model was extended into a 3D model in order to include the oblique waves. Model results verified the assumption made in Van Gent (2020) that the influence of oblique waves on the mean overtopping discharge depends on the berm width. The 3D numerical simulations are extremely computationally expensive. A single simulation for 200 s took three weeks to compute using 22 processors (2.7 GHz) in parallel. Thus, only one test was modelled for validation and one wave direction relative to the structure was simulated. Considering the 3D numerical model was used in a qualitative way, the model validation was regarded as being acceptable. Then, the same wave conditions and numerical settings for the validation test were enforced for other 3D simulations except that the berm was varied. Although the incident waves at the position of the wave gauge at loc10 are not or hardly affected by the side relaxation zones, the wave interaction at the structure in the sections between $z = 7$ m to 9 m could be affected by the side relaxation zones in the numerical wave basin with the reduced size. However, if this interference would be present, it existed for all the simulated cases and it is expected that the interference of incident waves has limited influence on the trend. Nevertheless, for more accurate predictions of the average overtopping discharge resulted from oblique waves, it is recommended to model the entire physical wave basin and to validate the 3D numerical model with more experimental data if the computational efficiency improves in the future. Additionally, the performance of the 3D numerical model can be further improved by using finer mesh. The sensitivity of mean overtopping discharges caused by perpendicular waves with the grid size was performed by Chen et al. (2020) which showed that finer mesh would lead to smaller mean overtopping discharges.

In the 3D numerical model, the flow characteristics were not analysed as no experimental data were available for validating the flow characteristics in three dimensions. It remains unknow how the oblique waves affect the flow velocity and layer thickness, which is recommended for future investigation.

6. Conclusion

Wave overtopping must be considered for the design and evaluation of coastal structures. The accurate estimates of overtopping flow parameters at the crest related to individual overtopping events are important for assessing the stability of the landward slope of dikes. The mean overtopping discharge is a key parameter in determining the crest level of dikes. Berms, roughness and oblique waves have significant effects on wave overtopping. Thus, their effects should be taken into account when predicting the wave overtopping process at dikes. This paper presents a numerical investigation of the effects of roughness, berm and oblique waves on wave overtopping processes at dikes. Both overtopping flow characteristics and the mean overtopping discharge were studied.

Ten tests selected from Van Gent (2002a) were used to validate the 2D OpenFOAM® model for predicting the overtopping flow velocity and layer thickness at the waterside edge of the dike crest. The spectral wave period was overestimated by the numerical model, which might be caused by the limitations of the OceanWave3D in dealing with the wave breaking and by the shorter simulation time of the numerical model. Further research on solving this problem is recommended. The model was shown to perform reasonably for simulating the flow characteristics. The validated model was then applied to investigate the effects of roughness and a berm on flow characteristics at the waterside edge of the crest. Model results show that if the roughness factor was excluded from the existing empirical Eqs. (1) & (2), the flow characteristics would be underestimated. Including the roughness factor as shown in Eqs. (1) & (2) leads to better estimates of flow velocities and layer thicknesses.

Thirty numerical tests were performed to study the berm influence on the flow velocity and layer thickness. Model results show that the flow parameters are sensitive to the berm width while they are not significantly influenced by the berm level. Existing empirical Eqs. (1) & (2) with coefficients by Van Gent (2002a) work well for estimating the flow parameters over the slopes with a berm. The berm influence was accounted for by the wave run-up height. It is recommended to use Eq. (A.1) to calculate the wave run-up height over slopes with a berm.

Distribution functions were derived based on the numerical model results for the flow velocity and layer thickness with exceedance probabilities below 10%. The extreme flow velocities follow a Rayleigh distribution function while the layer thickness follows a Weibull distribution function.

A 3D OpenFOAM® model was also developed to take the oblique waves into account by extending the 2D OpenFOAM® model into the 3D domain. Model results show that the influence of the oblique waves on the mean overtopping discharge depends on the berm width. It is recommended to investigate the effect of oblique waves in combination with a berm and/or roughness on the flow velocity and layer thickness.

CRediT authorship contribution statement

W. Chen: Writing – original draft, Software, Formal analysis, Conceptualization. **J.J. Warmink:** Conceptualization, Methodology, Writing – review & editing, Supervision. **M.R.A. van Gent:** Conceptualization, Resources, Writing – review & editing, Supervision. **S.J.M.H. Hulscher:** Conceptualization, Writing – review & editing, Supervision, Project administration.

Declaration of Competing Interest

The authors declare that they have no known competing financial interests or personal relationships that could have appeared to influence the work reported in this paper.

Acknowledgements

The first author thanks the China Scholarship Council for providing the research grant. This work is also part of the All-Risk research programme, with project number P15–21, which is partly financed by the Netherlands Organisation for Scientific Research (NWO). Joost den Bieman (Deltares) and Menno de Ridder (Deltares) are thanked for the valuable suggestions with respect to the OpenFOAM® modelling. This work was carried out on the Dutch national e-infrastructure with the support of SURF Cooperative.

Appendix A. Empirical formulas for wave run-up height

Van Gent (2001) developed empirical equations (A. 1) for estimating $R_{u2\%}$.

$$\frac{R_{u2\%}}{\gamma H_{m0}} = c_0 \xi_{m-1,0} \text{ for } \xi_{m-1,0} \le p$$

$$\frac{R_{u2\%}}{\gamma H_{m0}} = c_1 - c_2 \Big/ \xi_{m-1,0} \text{ for } \xi_{m-1,0} \ge p \quad \text{(A. 1)}$$

where c_0=1.35, c_1=4.7, $c_2 = 0.25c_1^2/c_0$ and $p = 0.5c_1/c_0$. H_{m0} [m] is the spectral significant wave height. γ [-] ($\gamma = \gamma_f \gamma_\beta$) is the reduction factor taking the influence of roughness (γ_f) and oblique wave attack (γ_β) into account. $\xi_{m-1,0}$ [-] ($\xi_{m-1,0} = \tan(\alpha)/\sqrt{\left(\frac{2\pi H_{m0}}{gT_{m-1,0}^2}\right)}$) is the Iribarren number. EurOtop (2018) also provide a method to estimate $R_{u2\%}$ as follows.

$$\frac{R_{u2\%}}{H_{m0}} = 1.65 \gamma_f \gamma_\beta \gamma_b \xi_{m-1,0} \quad \text{(A. 2)}$$

with a maximum of

$$\frac{R_{u2\%}}{H_{m0}} = 1.0 \gamma_f \gamma_\beta \left(4 - \frac{1.5}{\sqrt{\gamma_b \xi_{m-1,0}}}\right) \quad \text{(A. 3)}$$

where γ_b [-] is the influence factor of berms, which can be calculated using the following equations.

$$\gamma_b = 1 - r_B(1 - r_{dh}) \quad \text{if } 0.6 \le \gamma_b \le 1.0 \quad \text{(A. 4)}$$

Where r_B and r_{dh} are calculated using the following equations.

$$r_B = \frac{B}{L_{berm}} \quad \text{(A. 5)}$$

$$r_{dh} = 0.5 - 0.5\cos\left(\pi \frac{d_h}{R_{u2\%}}\right) \text{ for a berm above still water level} \quad \text{(A. 6)}$$

$r_{dh} = 0.5 - 0.5\cos\left(\pi \frac{d_h}{2H_{m0}}\right)$ for a berm below still water level where L_{berm} [m] is the characteristic berm length; d_h [m] is the berm level relative to the SWL;

Appendix B. Numerical data

Table B.1–Table B.3

Table B.1
Numerical (2DV) data of the roughness influence with protrusion height = 0.5 cm.

Test	h_toe	B [m]	H_{m0}_OF [m]	$T_{m-1,0}$_OF [s]	$h_{2\%}$_OF [m]	$u_{2\%}$_OF [m/s]	$R_{u2\%}$_OF [m]
R101	0.35	0	0.149	2.63	0.0205	1.51	0.358
R103	0.4	0	0.153	2.51	0.033	1.785	0.382
R104	0.45	0	0.149	1.98	0.034	1.6	0.31
R201	0.4	0	0.15	2.32	0.029	1.68	0.34
R202	0.4	0	0.148	2.23	0.0254	1.69	0.337
R203	0.4	0	0.138	2.14	0.0236	1.61	0.33
R204	0.4	0	0.127	2.14	0.022	1.44	0.315
R205	0.4	0	0.139	1.95	0.0179	1.35	0.282

Table B.2
Numerical (2DV) data of the berm influence.

Test	h_toe	B [m]	d_h [m]	H_{m0}_OF [m]	$T_{m-1,0}$_OF [s]	$h_{2\%}$_OF [m]	$u_{2\%}$_OF [m/s]	$R_{u2\%}$_OF [m]
T103	0.4	0	0	0.153	2.51	0.0326	1.91	0.406
W103b1	0.4	0.1	0	0.153	2.51	0.0312	1.85	0.39
W103b2	0.4	0.2	0	0.153	2.51	0.03	1.88	0.38
W103b3	0.4	0.3	0	0.153	2.51	0.0266	1.754	0.36
W103b4	0.4	0.4	0	0.153	2.51	0.0254	1.484	0.349
W103b5	0.4	0.5	0	0.153	2.51	0.0218	1.41	0.32
W103b6	0.4	0.1	0.1	0.153	2.51	0.0353	1.717	0.404
W103b7	0.4	0.1	0.05	0.153	2.51	0.0345	1.89	0.397
W103b8	0.4	0.1	−0.05	0.153	2.51	0.0318	1.92	0.402
W103b9	0.4	0.1	−0.1	0.153	2.51	0.0319	1.85	0.402
W103b10	0.4	0.3	0.1	0.153	2.51	0.0313	1.72	0.362
W103b11	0.4	0.3	0.05	0.153	2.51	0.0265	1.9	0.364
W103b12	0.4	0.3	−0.05	0.153	2.51	0.0274	1.54	0.362
W103b13	0.4	0.5	0.1	0.153	2.51	0.026	1.55	0.344
W103b14	0.4	0.5	0.05	0.153	2.51	0.0246	1.44	0.326
W103b15	0.4	0.5	−0.05	0.153	2.51	0.0218	1.33	0.321
W103b16	0.4	0.5	−0.1	0.153	2.51	0.0256	1.38	0.332
W201	0.4	0	0	0.15	2.32	0.029	1.85	0.372
W201b1	0.4	0.1	0	0.15	2.32	0.0271	1.77	0.364
W201b2	0.4	0.2	0	0.15	2.32	0.0255	1.7	0.342
W201b3	0.4	0.3	0	0.15	2.32	0.0235	1.42	0.33
W201b4	0.4	0.4	0	0.15	2.32	0.0193	1.28	0.306
W201b5	0.4	0.5	0	0.15	2.32	0.0172	1.24	0.298

Table B.3
Data for validation of the 2DV OpenFOAM® model.

Test	h_toe	H_{m0}_exp [m]	H_{m0}_OF [m]	$T_{m-1,0}$_exp [s]	$T_{m-1,0}$_OF [s]	$h_{2\%}$_exp [m]	$h_{2\%}$_OF [m]	$u_{2\%}$_exp [m/s]	$u_{2\%}$_OF [m/s]	$R_{u2\%}$_OF [m]
T101	0.35	0.149	0.149	2.16	2.63	0.0143	0.0217	1.53	1.66	0.391
T102	0.35	0.142	0.141	1.84	2.17	0.0058	0.0134	0.99	1.17	0.324
T103	0.4	0.153	0.153	2.14	2.51	0.0212	0.0326	1.74	1.91	0.406
T104	0.45	0.147	0.149	1.78	1.98	0.0204	0.0335	1.64	1.79	0.33
T201	0.4	0.152	0.15	2.03	2.32	0.016	0.029	1.55	1.77	0.372
T202	0.4	0.148	0.148	1.92	2.23	0.014	0.0265	1.53	1.75	0.362
T203	0.4	0.139	0.138	1.84	2.14	0.0117	0.0242	1.44	1.8	0.356
T204	0.4	0.13	0.127	1.86	2.14	0.0101	0.0244	1.29	1.65	0.348
T205	0.4	0.142	0.139	1.69	1.95	0.0076	0.0188	1.09	1.5	0.318
T206	0.4	0.138	0.134	1.62	1.89	0.0076	0.0184	1.08	1.43	0.305

References

Bouws, E., Günther, H., Rosenthal, W., Vincent, C.L., 1985. Similarity of the wind wave spectrum in finite depth water: 1. Spectral form. J. Geophys. Res. Ocean. 90, 975–986.

Capel, A., 2015. Wave run-up and overtopping reduction by block revetments with enhanced roughness. Coast. Eng. 104, 76–92. https://doi.org/10.1016/j.coastaleng.2015.06.007.

Chen, W., Marconi, A., Van Gent, M.R.A., Warmink, J.J., Hulscher, S.J.M.H., 2020. Experimental study on the influence of berms and roughness on wave overtopping at rock-armoured dikes. J. Mar. Sci. Eng. 8, 1–21. https://doi.org/10.3390/jmse8060446.

Chen, W., Van Gent, M.R.A., Warmink, J.J., Hulscher, S.J.M.H., 2020a. The influence of a berm and roughness on the wave overtopping at dikes. Coast. Eng. 156, 103613 https://doi.org/10.1016/j.coastaleng.2019.103613.

Chen, W., Warmink, J.J., Van Gent, M.R.A., Hulscher, S.J.M.H., 2021. Numerical modelling of wave overtopping at dikes using OpenFOAM®. Coast. Eng., 103890

Chen, W., Warmink, J.J., Van Gent, M.R.A., Hulscher, S.J.M.H., 2020b. Modelling of wave overtopping at dikes using openfoam. Coast. Eng. Proc. 27.

De Waal, J.P., van der Meer, J.W., 1992. Wave runup and overtopping on coastal structures. In: Proc. ICCE 1992. ASCE, pp. 1758–1771. https://doi.org/10.1016/B978-1-4160-5583-9.00134-9.

Dean, R.G., Rosati, J.D., Walton, T.L., Edge, B.L., 2010. Erosional equivalences of levees: steady and intermittent wave overtopping. Ocean Eng 37, 104–113. https://doi.org/10.1016/j.oceaneng.2009.07.016.

EurOtop, 2018. Manual on wave overtopping of sea defences and related structures, An overtopping manual largely based on European research, but for worldwide application. Van der Meer, J.W., Allsop, N.W.H., Bruce, T., De Rouck, J., Kortenhaus, A., Pullen, T., Schüttrumpf, H., Troch, P., Zanuttigh, B., www.overtopping-manual.com.

Formentin, S.M., Gaeta, M.G., Palma, G., Zanuttigh, B., Guerrero, M., 2019. Flow depths and velocities across a smooth dike crest. Water (Basel) 11, 2197.

Hughes, S., Scholl, B., Thornton, C., 2012. Wave overtopping hydraulic parameters on protected-side slopes. In: Proc. 32nd USSD Annu. Conf. Orleans,Louisiana, pp. 1453–1466.

Jacobsen, N.G., 2017. waves2Foam Manual.

Jacobsen, N.G., Fuhrman, D.R., Fredsøe, J., 2012. A wave generation toolbox for the open-source CFD library: openFoam®. Int. J. Numer. Methods Fluids 70, 1073–1088.

Larsen, B.E., Fuhrman, D.R., 2018. On the over-production of turbulence beneath surface waves in Reynolds-averaged Navier–Stokes models. J. Fluid Mech. 853, 419–460.

Mansard, E.P.D., Funke, E.R., 1980. The measurement of incident and reflected spectra using a least squares method. Coastal Eng. 154–172, 1980.

Mares-Nasarre, P., Argente, G., Gómez-Martín, M.E., Medina, J.R., 2019. Overtopping layer thickness and overtopping flow velocity on mound breakwaters. Coast. Eng. 154, 103561.

Mares-Nasarre, P., Molines, J., Gómez-Martín, M.E., Medina, J.R., 2021. Explicit Neural Network-derived formula for overtopping flow on mound breakwaters in depth-limited breaking wave conditions. Coast. Eng. 164, 103810.

Mayer, S., Garapon, A., Sørensen, L.S., 1998. A fractional step method for unsteady free-surface flow with applications to non-linear wave dynamics. Int. J. Numer. Methods Fluids 28, 293–315.

Paulsen, B.T., Bredmose, H., Bingham, H.B., 2014. An efficient domain decomposition strategy for wave loads on surface piercing circular cylinders. Coast. Eng. 86, 57–76.

Schoonees, T., Kerpen, N.B., Schlurmann, T., 2021. Full-scale experimental study on wave overtopping at stepped revetments. Coast. Eng. 167, 103887.

Schüttrumpf, H., 2001. Wellenüberlaufströmung an Seedeichen. Experimentelle und theoretische Untersuchungen. Braunschweig University.

Schüttrumpf, H., Oumeraci, H., 2005. Layer thicknesses and velocities of wave overtopping flow at seadikes. Coast. Eng. 52, 473–495. https://doi.org/10.1016/j.coastaleng.2005.02.002.

Schüttrumpf, H., Van Gent, M.R.A., 2003. Wave overtopping at seadikes. Coastal Struct. 431–443, 2003.

Suzuki, T., Altomare, C., Veale, W., Verwaest, T., Trouw, K., Troch, P., Zijlema, M., 2017. Efficient and robust wave overtopping estimation for impermeable coastal structures in shallow foreshores using SWASH. Coast. Eng. 122, 108–123.

TAW, 2002. Technical Report Wave Run-Up and Wave Overtopping At Dikes. Technical Advisory Committee on Flood Defence, Delft, The Netherlands.

Temmerman, S., Meire, P., Bouma, T.J., Herman, P.M.J., Ysebaert, T., De Vriend, H.J., 2013. Ecosystem-based coastal defence in the face of global change. Nature 504, 79.

Van Bergeijk, V.M., Warmink, J.J., Hulscher, S.J.M.H., 2020. Modelling the wave overtopping flow over the crest and the landward slope of grass-covered flood defences. J. Mar. Sci. Eng. 8 https://doi.org/10.3390/JMSE8070489.

Van Bergeijk, V.M., Warmink, J.J., van Gent, M.R.A., Hulscher, S.J.M.H., 2019. An analytical model for wave overtopping flow velocities on dike crests and landward slopes. Coast. Eng. 149, 28–38.

Van der Werf, I.M., Van Gent, M.R.A., 2018. Wave overtopping over coastal structures with oblique wind and swell waves. J. Mar. Sci. Eng. 6, 149.

Van Gent, M.R.A., 2021. Influence of oblique wave attack on wave overtopping at caisson breakwaters with sea and swell conditions. Coast. Eng. 164, 103834.

Van Gent, M.R.A., 2020. Influence of oblique wave attack on wave overtopping at smooth and rough dikes with a berm. Coast. Eng. 160, 103734.

Van Gent, M.R.A., 2019. Climate adaptation of coastal structures. In: Keynote in Proc. Applied Coastal Research (SCACR 2019).

Van Gent, M.R.A., 2002a. Low-exceedance wave overtopping events: measurements of velocities and the thickness of water-layers on the crest and inner slope of dikes. Delft Clust. DC1–322-3.

Van Gent, M.R.A., 2002b. Wave overtopping events at dikes. World Sci. ICCE 2002 2, 2203–2215. https://doi.org/10.1142/9789812791306.

Van Gent, M.R.A., 2001. Wave Runup on Dikes with Shallow Foreshores. J. Waterw. Port, Coastal, Ocean Eng. 127, 254–262. https://doi.org/10.1061/(ASCE)0733-950X(2001)127:5(254).